Faint Object Spectrograph On-Orbit Sky Background Measurements

R. W. Lyons, W. Baity, E. A. Beaver,
R. D. Cohen, V. T. Junkkarinen, J. B. Linsky
University of California San Diego

Instrument Science Report CAL/FOS-083
August 1992
Preliminary

I. Abstract

We present here the details of the sky background data obtained with the Faint Object Spectrograph in Science Verification proposals SV2965, SV2966 and SV2967. Sky light is an important contributor to several of the instrument configurations especially when the large science aperture is used. This data allowed us to derive some of the dependencies of the sky background on the telescope pointing direction.

II. Introduction

When observing targets with the Faint Object Spectrograph (FOS) aboard the Hubble Space Telescope (HST), background counts from the sky may be recorded, depending on the instrument configuration which is being used. In the UV the major sources of background light will be the N I (1200 Å), Ly α (1216 Å), and O I (1304 Å) emission lines from the ionosphere. Of these Ly α, the strongest, is expected to exceed N I, the weakest,by a factor of about 100 (Paresce and Volpe 1984). Diffuse galactic light (DGL) may also be a contributing source. In the optical, the major sources of sky background are expected to be the zodiacal light, diffuse galactic light, and especially at low galactic latitudes, individual faint stars. Various formulae are given in the FOS Instrument Handbook (Ford 1985, Ford and Hartig 1990) to estimate the contribution of the different sources to the FOS background.

Knowledge of the FOS sky background is necessary for several practical reasons. The FOS is equipped with burst noise rejection software. The software is activated by setting a parameter, REJLIM, equal to the total number of counts that must be received before an exposure frame is rejected. Since the sky background counts are included in this total it is necessary to know whether they are significant in order to avoid setting REJLIM so low that all the data are lost. For faint targets, it may be necessary to know the contribution of the sky background before setting the target detection limits in order to insure proper target acquisition. In some cases, knowledge of the sky background is necessary to reduce the data properly.

During Science Verification (SV) observations were made to investigate the character of the background light due to the position of the target. The observations were made under three test numbers:

SV2965 - high galactic latitude sky background test
SV2966 - low galactic latitude sky background test
SV2967 - low ecliptic latitude background.

Three configurations were tested. The G160L grating was used with the Blue and Red Digicons. The prism and G650L grating were used with the Red Digicon. The results of these tests are presented in this report. No sky background tests had been carried out previously during Orbital Verification.

III. Observations

Observation runs were made for both detectors under proposals SV2965, SV2966 and SV2967. The proposals did not indicate the specific areas of the sky that should be observed - instead they laid out criteria under which observations would be suitable. These criteria were designed so that the sky would be sampled at a number of positions at high and low galactic latitude and at low ecliptic latitude. When a verification test or science observation was completed and the conditions of scheduling permitted, the telescope was offset from the target just observed and sky readings were carried out using the FOS. In some cases, the OSS team noticed that the sky was not free of source light or other faint targets. The observation runs and the sky target areas are listed in chronological order by proposal and detector in Table I. The test specifications did not require that both detectors be used each time.

The exposures were made the same way for all the tests, but unlike other tests this differed for the two detectors. All exposures were made through the largest aperture, the $4''.3$ square also known as A-1. Spectra were taken in the normal manner - that is, they were quarter-stepped and overscanned so that the 512 diode array produced readouts of 2064 data values. Known problem channels were disabled. The ACCUM mode was used so that the array was only cleared after the last readout. Exposures were made only with the low dispersion configurations; on the Blue side the G160L was used, on the Red side the G160L, G650L and prism were used. Each configuration produced 3 files. For the Blue side, the first file consisted of one 300 second exposure, the second, two exposures totalling 600 seconds, and the third, three exposures totalling 900 seconds. For the Red side, the first file consisted of two exposures totalling 300 seconds, the second, 5 exposures totalling 600 seconds, and the third, 7 exposures totalling 900 seconds. The total exposure time must be divided by 4 to get the exposure time per pixel. Some of the runs occurred over more than one orbit but all the observations in any given file were made together.

Some of the high dispersion configurations are affected by sky light but these were not tested. In addition, no spectra were taken through the polarization filters.

IV. Data Reduction and Analysis

The geocoronal emission line intensity depends mainly on angular distance between the sun and the earth as seen from the HST (the sun-earth angle (SEA)) since this determines the illumination of the local atmosphere. For any given exposure, the intensity also depends on the angular distance between between the earth and the target as seen from the HST (the earth-target angle (ETA)) since this determines the path length through the atmosphere. The position of the sun (right ascension and declination) during the observation was obtained from the science header (SHH (the file extension)) file as was the angular distance between the sun and the target as seen from the HST (sun-target angle (STA)). Both of these do not change much during an observation. The position of the target was obtained from the SHH file. The right acension and declination of the earth relative to the HST at the time of the observation were computed from the orbital parameters in the SHH file using a program written by Tom Ake (HSTPOS), modified by Fred Walter and adapted locally for the FOS header format. This position was then used to compute the angular separation between the sun and the earth (SEA) and the earth and the target (ETA) at the time of the observation.

The individual spectra were extracted from the accumulated spectra after correcting the latter for the effects of the diodes disabled during the run. In each exposure, the mean dark background was determined by averaging the pixel counts in the regions clear of obvious features. The dark background was checked against that expected based on the results of the dark background test SV1316 (see Lyons *et al.* 1992). The few cases where there was a notable discrepancy involved intermittent noisy channels. Due to the way the exposure position was determined, the sky target was known to be contaminated in some instances. With the short exposure times used here, there was no evidence of contamination from faint sources. There did not appear to be any problem with scattered light.

For the G160L spectra taken with the Blue detector, mean count rates were determined for the peaks of the geocoronal lines. Only Lyα and O I λ1304 were measured; the N I line may be strong enough to have been detected but because the large aperture was used for all the exposures, it could not be separated from the nearby much stronger line of Lyα. The mean count rate in the first order spectrum excluding the geocoronal lines was also measured. The sun-earth angles, sun-target angles, and earth-target angles are listed in Table I of the Appendix together with the count rates for these regions. The peak of the zero order spectrum and the mean count rate in the first order spectrum were measured for the G160L observations made with the Red detector. These are presented in Table II of the Appendix. The mean value for the observed spectrum and the peak were found for both the G650L and prism spectra. For these observations, the galactic coordinates, determined using routines in the NOAO package in IRAF, and the ecliptic coordinates, determined from a short IDL routine, are were computed. (These are necessary to establish the dependence of the sky count rate on the zodiacal light and diffuse galactic background.) The positions and measures are listed in the Tables III and IV of the Appendix. The data in the Appendix is listed by exposure for the G160L runs and by file for the G650L and prism runs. The average count rate for the entire array is also listed for each entry in the tables. In some runs, the impact of noisy channels which had not been disabled is evident. All of the background count rates have been corrected for noisy channels; the count rates for the first order spectra taken with the G160L have also been corrected. None of the other rates have been adjusted. None of the count rates have been corrected for the background rate.

V. Appearance of the Sky Background

Sample plots of the type of data obtained for runs on the Red and Blue sides are presented in Figure 1. The full width at half maximum for all features that look like emission lines is 48 pixels. During OV it was determined that the spectrum, as imaged on the diode array, would wander slightly because of an interaction with the earth's magnetic field (Junkkarinen *et al.* 1990, Beaver and Foster 1992). The pixel positions indicated below have not been corrected for this effect which is much more pronounced with the Red detector than with the Blue one.

The output from the low resolution G160L configuration acquired with the Blue Digicon (Figure 1a) shows 4 features that appear like emission lines. Centered near pixel 624 is the zero order spectrum. Between pixels 1300 and 1400 are 2 geocoronal emission lines seen in the first order, Lyα (the stronger) centered on pixel 1319 and O I λ1304 centered on pixel 1369. Between these and the line-like feature centered near pixel 2012, actually second order Lyα, is the rest of the first order sky spectrum. Any sky light or target, accidentally present within the aperture, that produces a UV spectrum should be seen in this region. Weak emission from N I λ1200 may be evident in the blue wing of second order Lyα. Second order O I falls just off of the array. After several anomalously high average count rates caused by intermittent noisy channels were excluded, the maximum value for the count rate over the whole array in this data set was ~65 counts second^{-1}.

The output from the low resolution G160L configuration acquired with the Red Digicon (Figure 1b) shows one line-like feature. This is the zero order sky spectrum centered near pixel 1418. The faceplate on the Red Digicon strongly absorbs light shortward of 1700 Å so the geocoronal emission lines do not get imaged. This zero order spectrum should therefore result from a combination of zodiacal light, diffuse galactic background and any other relevant sources. The first order sky spectrum is recorded in the first 859 pixels. After excluding several anomalously high average count rates caused by intermittent noisy channels, the maximum count rate in this data set from the whole array was ~75 counts second^{-1}.

The output from the low resolution G650L configuration acquired with the Red Digicon (Figure 1c) shows several features. The plot of counts versus channel show a line like feature near pixel 1414. This is the zero order spectrum. The first order spectrum is the relatively smooth curve between 3500 and 7100 Å. The HST-FOS efficiency curve indicates that the G650L grating has close to 0 efficiency short of 3500 Å(Kinney 1992). A red tail which becomes noticeable long of 7100 Å is due to overlap from the second order spectrum.

The sources for this spectrum should be the same as those which contribute to the G160L Red detector spectra. For the data available, the mean count rate from the entire array peaks near 80 counts second $^{-1}$. Coincidentally, the mean count rate in the zeroth order spectrum turned out to be very similar to the mean count rate for the first 859 pixels (the first and second order spectra).

The Red Digicon with the prism is sensitive over a slightly larger range (1850-8950 Å) than with the G650L but the sky spectrum (Figure 1d) is very similar, a smooth curve running between 3000 and 9000 Å. (Note that the readout when the prism is used is opposite that when the gratings are used.) The sources producing this spectrum should be the same. The FOS efficiency curves (Kinney 1992) indicate that the prism configuration is ~3 times more efficient than the G650L configuration. While the count rate difference at the peak is greater than this factor would indicate, the spectra are compatible with what one would expect when allowance is made for the rapidly decreasing dispersion of the prism at longer wavelengths. For this data set, the highest average count rate obtained from the entire array was almost 150 counts second^{-1}.

VI. Positional Dependence of the Sky Count Rate

The expected relationship between sky background sources and the Digicon count rate at the peak (N_λ) is presented in Table 4.3-1 of the FOS Instrument Handbook version 1 (Ford 1985, Ford and Hartig 1990) and reproduced in Table II for convenience. In these formula, E_λ is the combined HST+FOS efficiency for the grating configuration of interest. *Ap* refers to the aperture area in square arc seconds. Unlike most of the other apertures available with the FOS, the 4.''3 square aperture used during these tests is considerably larger in size than an individual diode. The effective aperture for these tests thus becomes 4.''3 by 1.''4 since the diodes are only 1.''4 high. The zodiacal light is a function of the heliocentric ecliptic longitude and the ecliptic latitude (Levasseur-Regourd and Dumont 1980). The formula shown here approximates the solar spectrum source function with a Planck distribution of 5770° K. The diffuse galactic light is a function of b, the galactic latitude. The tabular information necessary to use these formulae is presented in Table II but one will need to consult the Handbook (Kinney 1992) for the relevant efficiency functions.

VI-1. The Geocoronal Lines - Lyα and O I

Figures 2 and 3 show the change in the measured intensities of the geocoronal line Lyα and O I λ1304 as a function of the sun-earth angle - 0° corresponds to HST midnight (sun behind the earth) and 180° corresponds to HST noon (HST between the sun and the earth). The mean count rate was measured across 36 pixels centered on the expected wavelengths; this was then adjusted for the background count rate using the the mean background near the lines. Lyα is always present, producing a minimum count rate of about 0.2 c/s/d at midnight and a maximum about 2 c/s/d at noon. O I is somewhat more sensitive to the sun's relative position, being essentially zero for sun-earth angles less than 80°. (Henceforth this position angle is used to denote the angle for the transition between day and night.) The count rate for O I is slightly higher, and on one run considerably higher, than one would expect based on the intensities found in Table II. Second order Lyα is approximately half the strength of the first order feature while second order O I falls just off the array.

There is a considerable spread in the count rates at any given sun-earth angle. Examination of the positional information indicates that, for a given run (6 exposures), the sun-target angles (total range for all runs 50-180°) do not change by much. The sun-earth angles and the earth-target angles (total range from all runs 70-180°) often undergo considerable change especially when the run is spread over more than one orbit. (The ranges represented by the data in a given file depend on the total exposure time for the file.) There is a strong tendency, particularly when the atmosphere is well illuminated, for observations at smaller earth-target angle to have a higher count rate. There is a weak tendency for observations with smaller sun-target angles to have a higher count rate. This latter result is not as convincing because there are few data points at high sun-target angles. It appears that at least some the scatter is intinsic, perhaps due to changing conditions in the Earth's upper atmosphere.

Similar behaviour for geocoronal Lyα was found by Fred Walter (1990,1991) from data obtained with the GHRS.

Table II includes a formula for calculating the count rate for the airglow lines. The efficiency of the configuration at Lyα is $\sim$1.1x10^{-3}. The count rates predicted (1.75 at noon and 0.2 at midnight) are similar to those found observationally. For O I, the efficiency is $\sim$2.5 x10^{-3}. The predicted count rate at noon, 0.38 c/s/d, is slightly lower than the bulk of this data would indicate.

VI-2. The Zodiacal Light and Diffuse Galactic Background

These backgrounds are harder to quantify than the single emission lines discussed in the previous section. In order to do this, a small number of pixels (96 for the G650L and 24 for the prism) near the wavelength of peak intensity have been averaged together. The average count rate in the closest nearby background region has also been determined. The background adjusted average count rate at the peak intensity has been plotted in Figures 4 through 7. In these figures, there is one point for each file from a run - since each run produces 3 files the points appear to cluster. The data are tabulated by file (i.e. all the exposures from a given file have been averaged together) in Appendix Tables III and IV.

Figures 4 and 6 present the data from the G650L and the prism as if it were due to zodiacal light. Zodiacal light depends on the angular separation between the target and the sun along the ecliptic (heliocentric ecliptic longitude) and the distance above the ecliptic. The angular separation can be, at most, 180°. In the top diagram of each of these figures, different symbols have been used to indicate three different ecliptic latitude ranges. Because points near the galactic plane may be affected by diffuse galactic light, points at low galactic latitude have been marked further by overplotting them with another symbol. The relationship between zodiacal light and the background count rate is not well defined.

Figures 5 and 7 present the data as if it were due to diffuse galactic light. Diffuse galactic light depends on the position of the target relative to the galactic center and can be characterized through the use of galactic coordinates. The galactic center is at the origin and longitude is specified running along the galactic plane. In the top diagram of each of these figures, different symbols have been used to indicate three different galactic latitude ranges. As the sky target gets farther from the galactic plane this component should become very small. Because points near the plane of the ecliptic may be affected by zodiacal light, points at low ecliptic latitude have been marked further by overplotting them with another symbol. The expected relationship between the diffuse galactic light and the background count rate is not apparent.

If the only correlations were with zodiacal light and/or diffuse galactic light we would expect that all the observations in any given run would produce similar, if not the same, average count rates. The large discrepancies that exist in many of the runs indicate that some additional factors are necessary to characterize the sky background variation. In the lower diagrams in Figures 3 through 7 the corresponding data are plotted with symbols that indicate sun earth angles (SEA) $\leq 80^o$ (designated as HST night) and $>80^o$ (designated as HST daytime). It is immediately apparent that, in all but one case (and the difference here is small), the lowest measure for any run in which a nightime-daytime change took place was taken at the smaller SEA. Most of the high count rates were obtained during the daytime. We conclude that the sun, perhaps through scattered sunlight, has a major impact on the background sky light especially during daytime observations. Figure 8 shows the count rates plotted against SEA. This figure does show the expected correlation but there is a lot of scatter. This is not surprising - some of the measures show very little difference while others change by factors of $\sim$2-3 over short time scales. Some other factors must be involved.

Before looking for the effect of the zodiacal light, we must throw out all of the daytime observations. When this is done, there is a *tendency*, as expected, for the sky background rate to increase as the difference in ecliptic longitude between the sun and the target decreases. When the ecliptic latitude is small the count rate appears to be higher, as expected, but this statement really rests on little data. When we throw out all the daytime observations, conclusions about any effects from diffuse galactic light are more tentative. For these data sets, only observations between galactic longitudes 60^o and 180^o lie far enough away from the plane of the ecliptic that zodiacal light is not a potential contributor. There may be some variation but the scatter is large. The data are insufficient to firmly establish either correlation. Patchiness in either source should not be overlooked as a possible cause of some of the scatter between points from different runs.

Models of the sky spectrum expected from the zodiacal light and the diffuse galactic background were computed for both instrument configurations using the equations in Table II. The efficiency functions were supplied by Don Neill (priv. comm.). The functions, appropriately converted and scaled so that the peak values matched those shown by Kinney (1992), are shown in Figure 9. They differ in detail from those shown by Kinney (1992) but are sufficient for our purposes. The predicted sky spectra are shown in Figures 10 and 11. At its maximum, the count rate expected from the zodiacal light falls in the midrange for this data. Almost all the count rates lie above the maximum count rate expected from the diffuse galactic background. Considering the short term scatter one might legitimately wonder how many of the counts recorded actually arise from either source.

VII. Conclusions and Recommendations.

We find that there is considerable short term variation in the strength of the features seen when one exposes on "blank" sky. We speculate that this is due scattered sunlight, or some other factor(s) related to the sun (e.g. the level of solar activity) producing changes in the earth's upper atmosphere.

For the G160L operating with the Blue detector, the strengths of the geocoronal lines correlate well with the the sun-earth angle. The strength of Lyα agreed well with the predictions. It is always present at some level but can be minimized by observing at small sun-earth angles. The O I line proved to be slightly stronger, but in some cases much stronger, than expected. There is some indication for considerable short term time-dependence in the O I count rate. Interference from geocoronal O I can be effectively eliminated by observing at sun-earth angles $\leq 80^o$. In addition, while not as effective, the count rate from both these lines can be reduced by observing at high earth-target angles. In these tests, N I was not a noticeable geocoronal line.

With the data that has been obtained so far for the G650L and prism operating with the Red detector, there is no firm evidence to suggest that there has been a definite detection of either the zodiacal light or the diffuse galactic background. While detection may be complicated by patchiness in the diffuse galactic background or time dependence of the zodiacal light, the large short period variation that has been observed in these tests suggests at least one other source is responsible for a significant fraction of the flux observed. There is a correlation between the count rate and thc position of the sun but there appears to be at least one other factor involved. Observers using these configurations will need to assess the impact of these uncertainties on their programs for themselves. Bear in mind that these tests were run with the largest FOS aperture.

Allowances will need to be made by anyone using the burst noise rejection software. If the slit is not small enough or the relevant diodes are not disabled, great care will need to be taken to avoid setting the rejection parameter, REJLIM, too low and therefore loosing all the data. We recommend exploration of an observing strategy in which diodes affected by the geocoronal lines or other narrow features can be selectively added to the disabled diode table temporarily for observers who wish to take advantage of the burst noise rejection option. With the current observing procedures an observer can at best specify a limited range of diodes that can be active. Activating REJLIM will cost the observer any background information or spectrum that might be available outside of that range.

Unfortunately all tests were run with the large aperture. The small apertures can be obtained by scaling the results but some small aperture tests to verify this scaling would be in order. Some tests with the polarizing filters might prove fruitful.

VII. Acknowledgements.

The authors would like to thank Fred Walter for supplying copies of his GHRS work on the geocoronal Lyα line and copies of his software.

Note Added In Proof

At the conclusion of this work, it was realized with a certain amount of chagrin that a large portion of the available data had been inadvertently left out of the analysis. Some of this new data was taken after changes were made in the key words in the header files. Changes will need to be made to the reduction and analyses programs to handle all the data.

While it is not expected to change any of the conclusions derived herein, this report must at this time be considered preliminary.

References.

Beaver, E. and Foster, P. 1992 "Lab Test Results of the FOS Detector Performance in a Variable External Magnetic Field", CAL/FOS-082.

Ford, H. 1985 "Faint Object Spectrograph Instrument Handbook - Version 1", published by Space Telescope Sciences Institute Oct. 1985.

Ford, H., Hartig, G. 1990 "Faint Object Spectrograph Instrument Handbook - Version 1.1", published by Space Telescope Sciences Institute May 1990.

Junkkarinen V., Cohen, R., Hier, R., Loyns, R., Rosenblatt, E. 1990 "Geomagnetic Image Deflection Problem in the FOS", CAL/FOS-066.

Kinney, A. 1992 "Hubble Space Telescope Faint Object Spectrograph Instrument Handbook - Version 2", published by Space Telescope Science Institute April 1992.

Levasseur-Regourd, A.C., Dumont, R. 1980, *Astron. Astrophys.*, **84**, 277.

Lyons, R. W., Baity, W. A., Beaver, E. A., Cohen, R. D., Junkkarinen, V. T., Linsky, J. B., and Rosenblatt, E.I. 1992 "Faint Object Spectrograph On-Orbit Dark Background Measurements", CAL/FOS-080.

Paresce, F. and Volpe, R. 1984 "The Background Radiation Model for the Space Telescope"

Walter, F. M. 1990 "The GHRS Spectrum of Geocoronal Lyman α", GHRS Cal/SV Report, 30 Oct.

Walter, F. M. 1991 "Further Measurements of the Geocoronal Background", GHRS Cal/SV Report, 30 Jan.

Table IA: Listing of Sky Background Runs for FOS Red Detector.

Chronological Listing of FOS 2965 Files

File Root	Date	Sky Target	File Root	Date	Sky Target
Y0G124	25/02/91	BKG-NGC4478	Y0G11C	25/08/91	BKG-HD6767
Y0G121	28/02/91	BKG-HD93521	Y0G118	12/10/91	BKG-HD2880
Y0G129	22/03/91	BKG-GRW+70D5824	Y0G12B	27/10/91	BKG-HD120787
Y0G126	23,30/03/91	BKG-SAO16291	Y0G11T	27/10/91	BKG-NGC2903
Y0G122	25/05/91	BKG-HZ21	Y0G11D	02/11/91	BKG-HD8382
Y0G11P	26/05/91	BKG-BD+75D325	Y0G11Y	08/11/91	BKG-SA101-363
Y0G12D	13/06/91	BKG-HD124973	Y0G11V	08/11/91	BKG-SA101-88
Y0G12E	13/06/91	BKG-PG1422+028	Y0G11X	23/11/91	BKG-SA101-207
Y0G11B	22/06/91	BKG-BPM16274	Y0G11Q	01/12/91	BKG-HD72905
Y0G11W	28/06/91	BKG-SA101-330	Y0G11S	01/12/91	BKG-A+81D266
Y0G11R	29/06/91	BKG-SAO6790	Y0G11U	01/12/91	BKG-HD84737
Y0G111	02/07/91	BKG-SA113-339	Y0G11A	08/12/91	BKG-NGC246
Y0G11O	07/07/91	BKG-30DOR	Y0G11L	28/12/91	BKG-HZ4
Y0G11F	10/07/91	BKG-HD16620	Y0G11Z	29/12/91	BKG-PKS0955+326
Y0G12M	15/07/91	BKG-SA113-442	Y0G120	29/12/91	BKG-HD89309
Y0G125	12/08/91	BKG-BD+29D2335	Y0G12I	29/12/91	BKG-SAO16956
Y0G12C	14/08/91	BKG-HD124897	Y0G12H	08/01/92	BKG-SA107-351
Y0G11M	15/08/91	BKG-SA95-233	Y0G12G	09/01/92	BKG-SA107-452
Y0G119	25/08/91	BKG-HD3823	Y0G128	12/01/92	BKG-HZ44

Chronological Listing of FOS 2966

File Root	Date	Sky Target	File Root	Date	Sky Target
Y0G20W	04/03/91	BKG-HD93204	Y0G20S	15/10/91	BKG-AI-VEL
Y0G20Y	05/03/91	BKG-ETA-CARINAE	Y0G20U	12/10/91	BKG-IOTACARINA-270
Y0G202	11/07/91	BKG-HD11408	Y0G20S0	15/10/91	BKG-AI-VEL
Y0G204	11/07/91	BKG-HD20135	Y0G2060	24/11/91	BKG-SAO13012
Y0G220	26/07/91	BKG-V1016CYG	Y0G20A0	06/12/91	BKG-STEIN-2051A
Y0G222	26/07/91	BKG-CYG-XR-1	Y0G20C0	07/12/91	BKG-CRAB-NEBULA
Y0G224	26/07/91	BKG-NGC6853	Y0G20E0	07/12/91	BKG-NGC1952
Y0G208	27/08/91	BKG-CK1-1			

Chronological Listing of FOS 2967

File Root	Date	Sky Target	File Root	Date	Sky Target
Y0G302	26/07/91	BKG-H-II-1776	Y0G324	27/10/91	BKG-HD89309
Y0G30I	27/07/91	BKG-PMT-DARK-SKY	Y0G3260	05/12/91	BKG-3C273
Y0G328	27/07/91	BKG-3C279	Y0G31K0	07/12/91	BKG-CRAB-PULSAR
Y0G304	30/09/91	BKG-LB227	Y0G31I0	07/12/91	BKG-NGC1952
Y0G322	01/10/91	BKG-AO0235+164	Y0G31M0	08/12/91	BKG-LAT-COL-1A
Y0G306	05/10/91	BKG-VA310	Y0G31G0	08/12/91	BKG-CRAB-NEBULA
Y0G308	21/10/91	BKG-VA622	Y0G30A0	12/01/92	BKG-NGC2392

Table IB: Listing of Sky Background Runs for the FOS Blue Detector.

Chronological Listing of FOS 2965 Files

File Root	Date	Sky Target	File Root	Date	Sky Target
Y0G10N	24/02/91	BKG-NGC4478	Y0G10U	17/06/91	BKG-SA107-452
Y0G10K	28/02/91	BKG-HD93521	Y0G10V	17/06/91	BKG-SA107-351
Y0G10O	23/03/91	BKG-SAO16291	Y0G10J	27/06/91	BKG-SA101-330
Y0G10L	25/03/91	BKG-HZ21	Y0G111	28/06/91	BKG-SA113-339
Y0G10M	01/05/91	BKG-HZ44	Y0G111	28/06/91	BKG-SA113-342
Y0G10E	02/05/91	BKG-BD+75D325	Y0G10Y	07/07/91	BKG-HR6636
Y0G106	25/05/91	BKG-HD8391	Y0G110	15/07/91	BKG-SA113-442
Y0G102	25/05/91	BKG-NGC246	Y0G112	15/07/91	BKG-HD213220
Y0G103	02/06/91	BKG-BPM16274	Y0G113	10/08/91	BKG-HD215405
Y0G104	02/06/91	BKG-HD6767	Y0G10B	15/08/91	BKG-SA95-52
Y0G10G	03/06/91	BKG-SAO6790	Y0G116	18/08/91	BKG-HD216435
Y0G10F	07/06/91	BKG-HD72905	Y0G115	25/08/91	BKG-HD216009
Y0G10I	07/06/91	BKG-HD84737	Y0G10W	29/09/91	BKG-SAO16956
Y0G10T	10/06/91	BKG-SA107-990	Y0G10X	30/09/91	BKG-HD155103
Y0G10P	12/06/91	BKG-NGC5033	Y0G10H	18/10/91	BKG-NGC2903
Y0G107	12/06/91	BKG-HD16620	Y0G15D	02/11/91	BKG-30DOR
Y0G10R	17/06/91	BKG-HD124973	Y0G15C	05/11/91	BKG-NGC1850
Y0G10S	17/06/91	BKG-PG1422+028			

Chronological Listing of FOS 2966

File Root	Date	Sky Target	File Root	Date	Sky Target
Y0G20V	04/03/91	BKG-HD93204	Y0G20P	25/08/91	BKG-ZETAPUP
Y0G20X	04/03/91	BKG-ETA-CARINAE	Y0G203	27/08/91	BKG-HD20135
Y0G223	14/04/91	BKG-NGC6853	Y0G20T	30/08/91	BKG-IOTACARINA-270
Y0G229	21/04/91	BKG-LAMBDA-CEP	Y0G207	01/09/91	BKG-CK1-1
Y0G227	25/04/91	BKG-NGC6995	Y0G20D	13/09/91	BKG-NGC1952
Y0G20N	01/05/91	BKG-NGC2440	Y0G20F	20/09/91	BKG-CRAB-PULSAR
Y0G21X	08/07/91	BKG-HMSGE	Y0G20Z	30/10/91	BKG-PCEN3532
Y0G201	10/07/91	BKG-HD11408	Y0G20B	06/11/91	BKG-CRAB-NEBULA
Y0G21V	11/07/91	BKG-VYS65-B	Y0G205	10/11/91	BKG-SAO13012
Y0G20L	24/08/91	BKG-R-MON	Y0G20J	12/12/91	BKG-LAT-COL-1A

Chronological Listing of FOS 2967

File Root	Date	Sky Target	File Root	Date	Sky Target
Y0G30L	21/06/91	BKG-S118	Y0G31J	20/09/91	BKG-CRAB-PULSAR
Y0G307	23/07/91	BKG-VA622	Y0G301	30/09/91	BKG-H-II-1776
Y0G30H	27/07/91	BKG-PMT-DARK-SKY	Y0G323	27/10/91	BKG-HD89309
Y0G303	03/09/91	BKG-LB227	Y0G325	24/11/91	BKG-3C273
Y0G305	05/09/91	BKG-VA310	Y0G309	09/01/92	BKG-NGC2392
Y0G31H	05/09/91	BKG-NGC1952	Y0G329	09/01/92	BKG-HD124973
Y0G321	06/09/91	BKG-AO0235+164			

Table II: Sky Light Sources

Airglow

$$N_\lambda = 84.6 I(KR) E_\lambda f(Ap)$$
$$f(Ap) = 0.7Ap, \sqrt{Ap} \leq 0.35''$$
$$f(Ap) = 0.35\sqrt{Ap}, \sqrt{Ap} > 0.35''$$

Airglow Emission Line Intensities at the ST Zenith

λ(Å)	Element	I(KR) ST Midnight	I(KR) ST Noon
1200	NI	-	0.22
1216	HI	2.5	22
1304	OI	-	2.1

Zodiacal Light

$$N_\lambda = 3.6 \times 10^{24} \frac{\triangle\lambda E_\lambda Ap 10^{-0.4M_v}}{\left(e^{24936/\lambda(\mathring{A})} - 1\right)\lambda^4(\mathring{A})}$$

Zodiacal Light Sky Brightness, M_v

	Ecliptic Latitude			
$\lambda - \lambda_\odot$	0	30	60	90
180	22.1	22.7	23.2	23.3
145	22.4	22.9	23.3	23.3
110	22.3	22.9	23.3	23.3

Diffuse Galactic Light

$$N_\lambda = 4.2 \times 10^4 f(\lambda) \triangle\lambda E_\lambda Ap$$
$$f(\lambda) = \{1.766 \times 10^{-6} - 1.765 \times 10^{-9}\lambda$$
$$+5.613 \times 10^{-13}\lambda^2 - 4.984 \times 10^{-17}\lambda^3\} e^{t_\lambda b}, \lambda \leq 4250 \text{ Å}$$
$$f(\lambda) = \frac{3.48 \times 10^{10} e^{t_\lambda b}}{(e^{22221/\lambda} - 1)\lambda^4}, \lambda > 4250 \text{ Å}$$
$$t_\lambda = -1.14 \times 10^{-2} - 1.0376 \times 10^{-5}\lambda$$

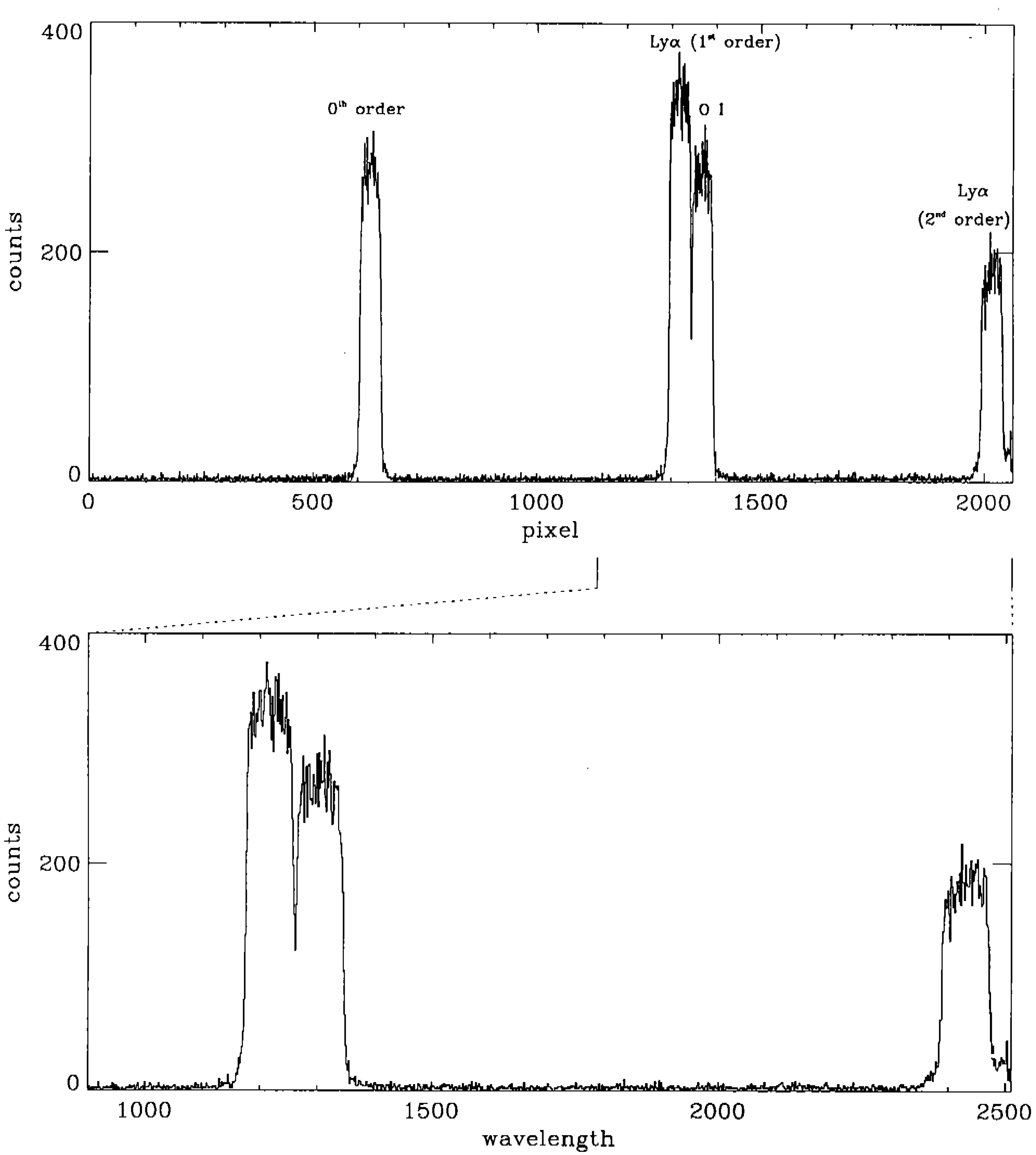

Figure 1a: Sample Sky Background – Blue Digicon with G160L.

File Y0G10003R, a 900 second exposure through the A–1 aperture, is shown above in pixel and wavelength space. Wavelengths are not available for all pixel positions. The exposure per pixel is 225 seconds.

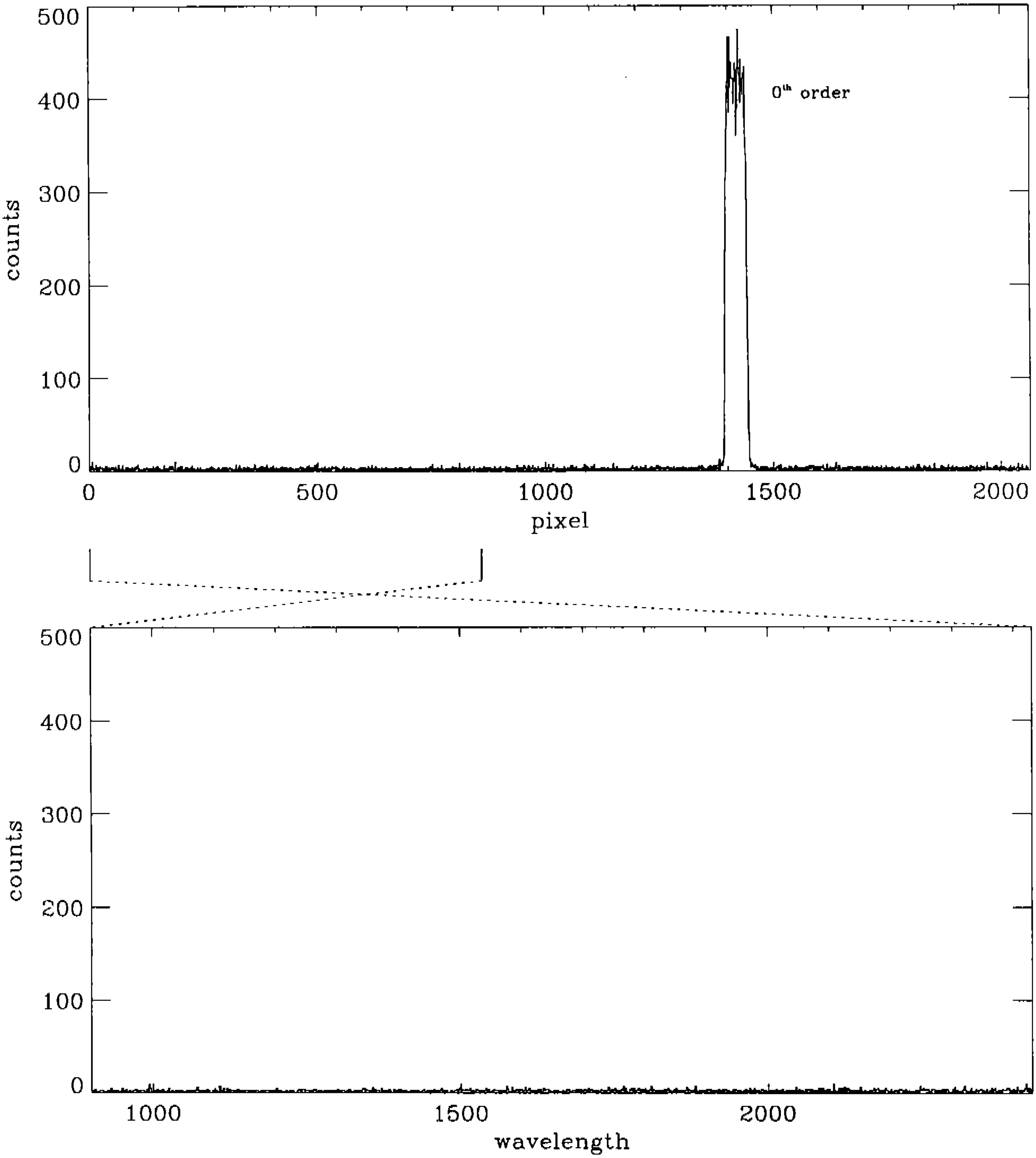

Figure 1b: Sample Sky Background – Red Digicon with G160L.

File Y0G12403T, a 900 second exposure through the A–1 aperture, is shown above in pixel and wavelength space. Wavelengths are not available for all pixel positions. The exposure per pixel is 225 seconds.

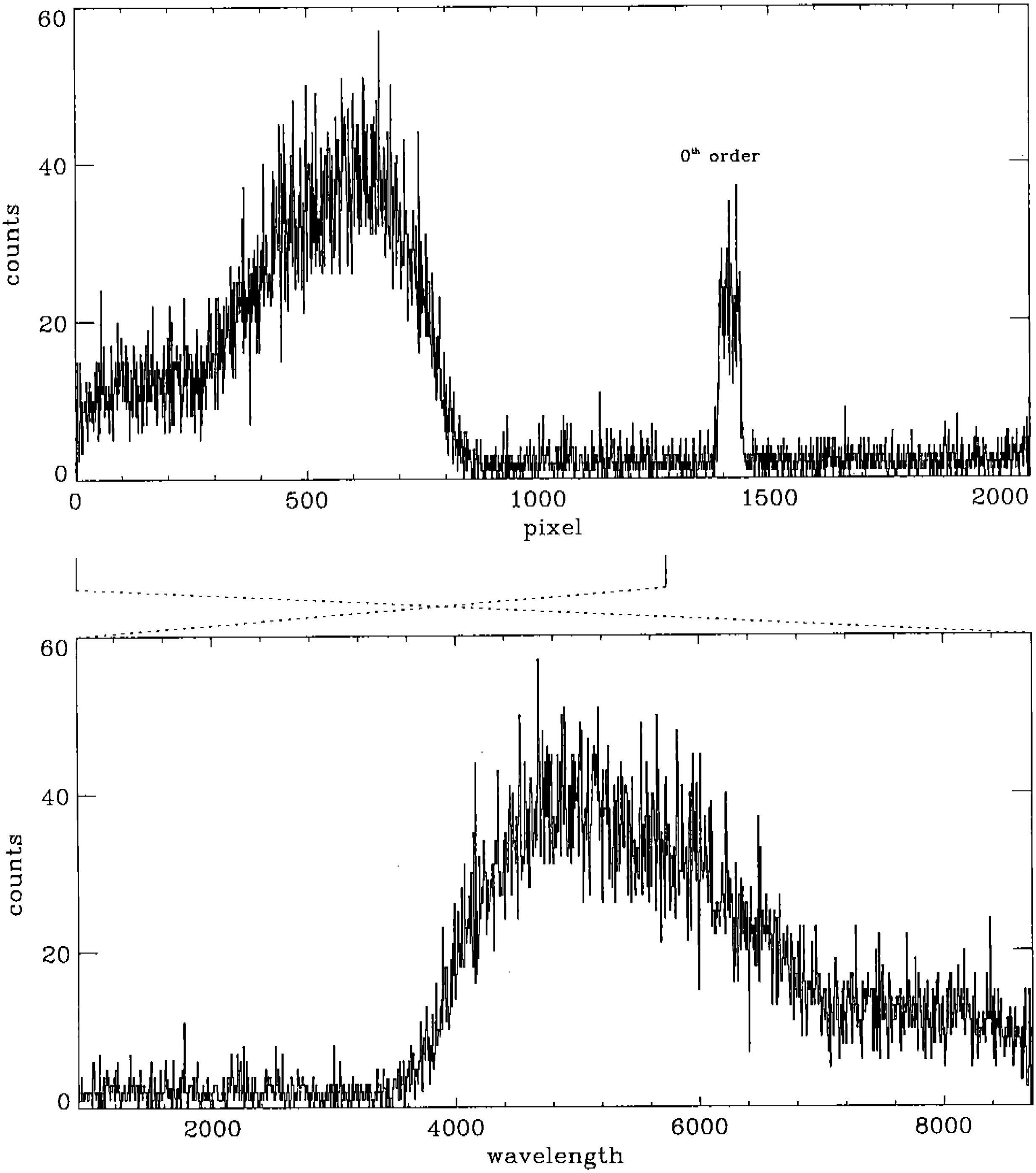

Figure 1c: Sample Sky Background – Red Digicon with G650L.

File Y0G12406T, a 900 second exposure through the A–1 aperture, is shown above in pixel and wavelength space. Wavelengths are not available for all pixel positions. The exposure per pixel is 225 seconds.

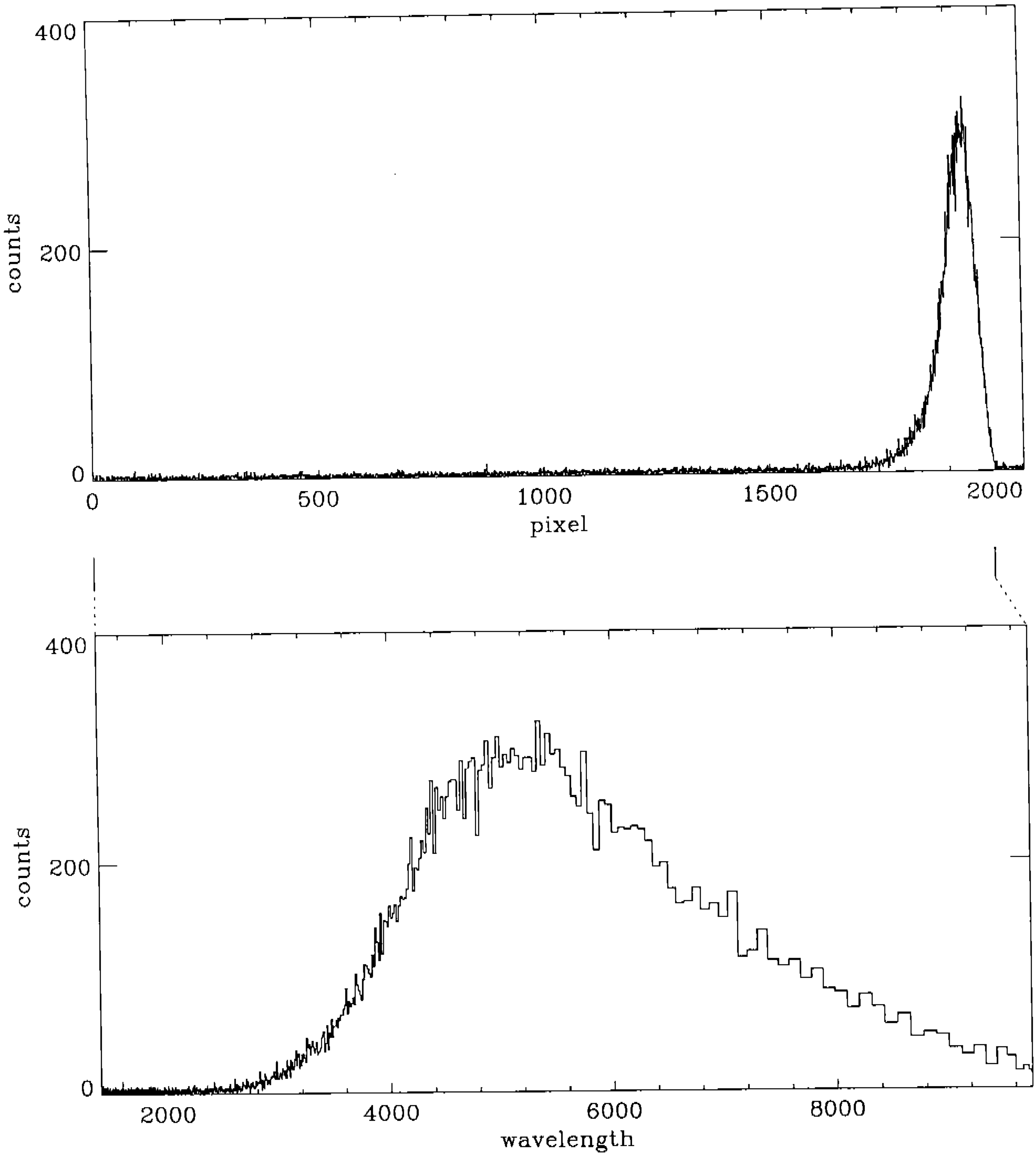

Figure 1d: Sample Sky Background – Red Digicon with Prism.

File Y0G12409T, a 900 second exposure through the A–1 aperture, is shown above in pixel and wavelength space. Wavelengths are not available for all pixel positions. The exposure per pixel is 225 seconds.

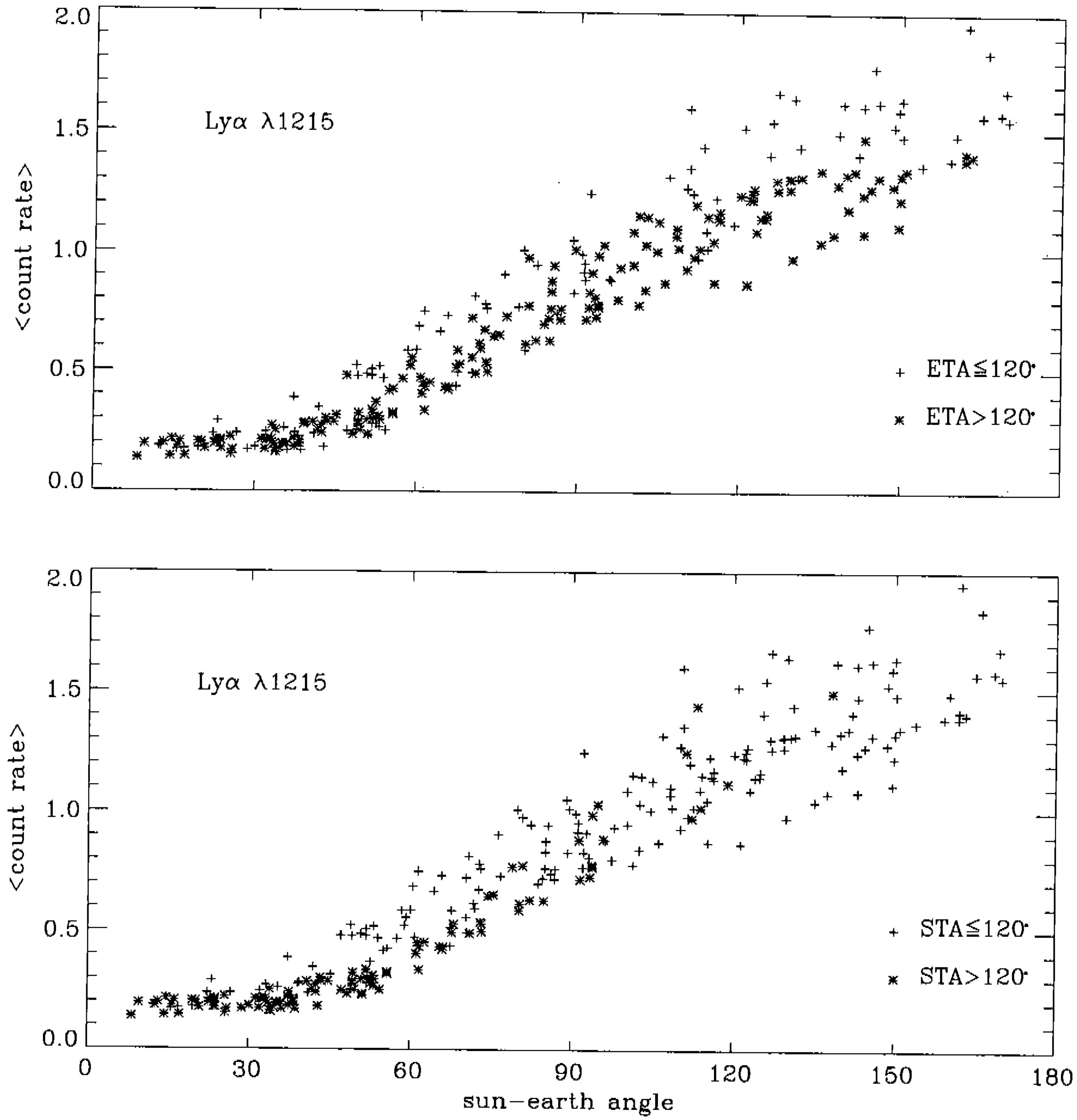

Figure 2: Relationship Between Position and Lyα Count Rate.

The average count rate at the peak of the geocoronal line Lyα is plotted against the angle between the sun and the earth as seen from the spacecraft. 180 degrees corresponds to solar noon. The different symbols indicate observations at different earth target and sun target angles. All the numbers are taken from the G160L results with the Blue detector. The effects of the background have been removed.

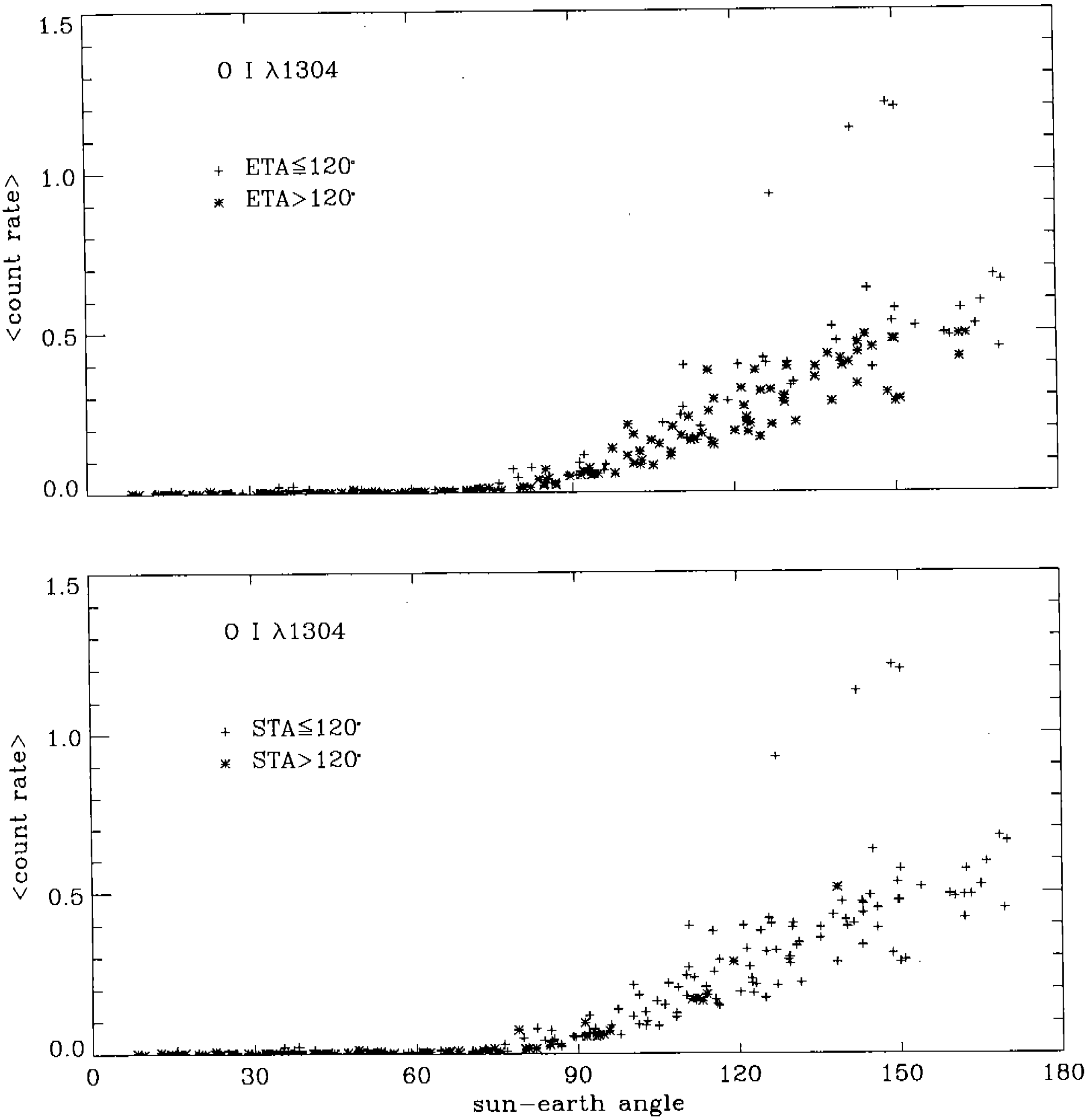

Figure 3: Relationship Between Position and O I λ1304 Count Rate.

The average count rate at the peak of the geocoronal O I line is plotted against the angle between the sun and the earth as seen from the spacecraft. 180 degrees corresponds to solar noon. The different symbols indicate observations at different earth target and sun target angles. All the numbers are taken from the G160L results with the Blue detector. The effects of the background have been removed.

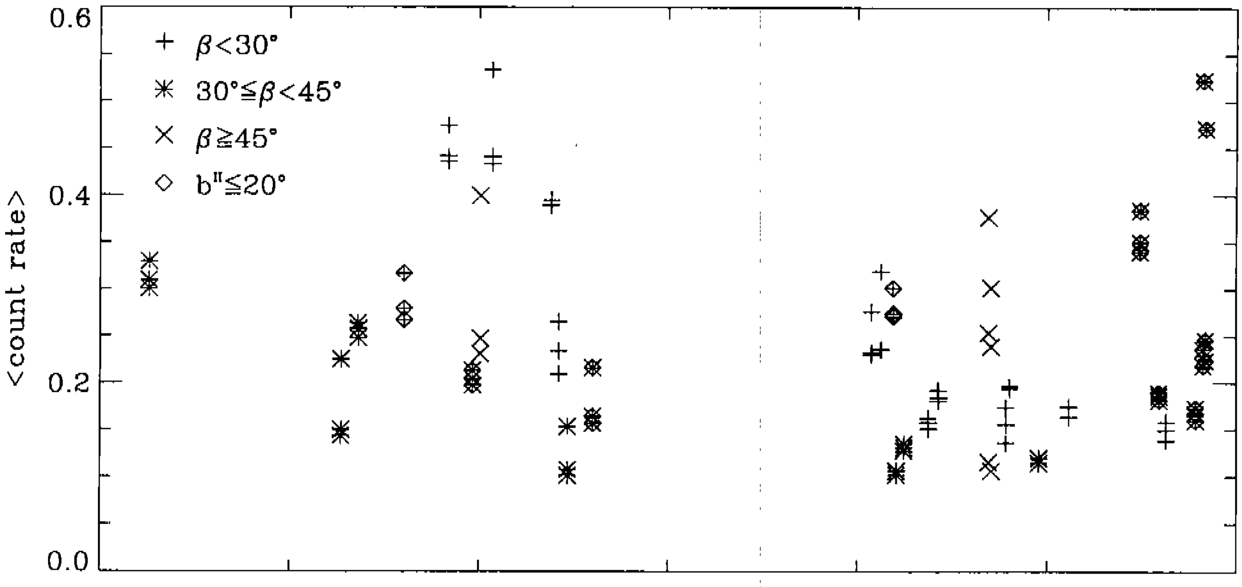

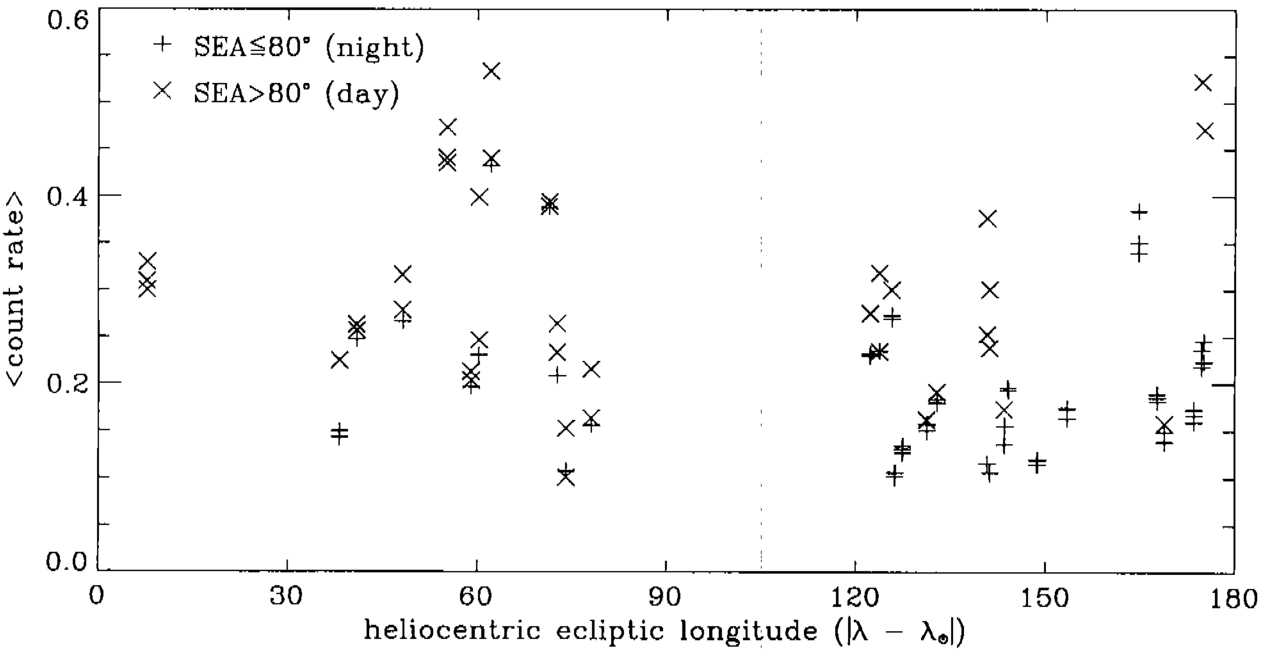

Figure 4: Relationship Between G650L Sky Count Rate and Zodiacal Light.

The average count rate at the peak of the sky spectrum taken with the G650L disperser and the Red Digicon is plotted against the difference in ecliptic longitude between the sun and the target. In the top figure different symbols are used to designate different ecliptic latitudes. The correlation between count rate and the time of day aboard the spacecraft is shown in the bottom diagram.

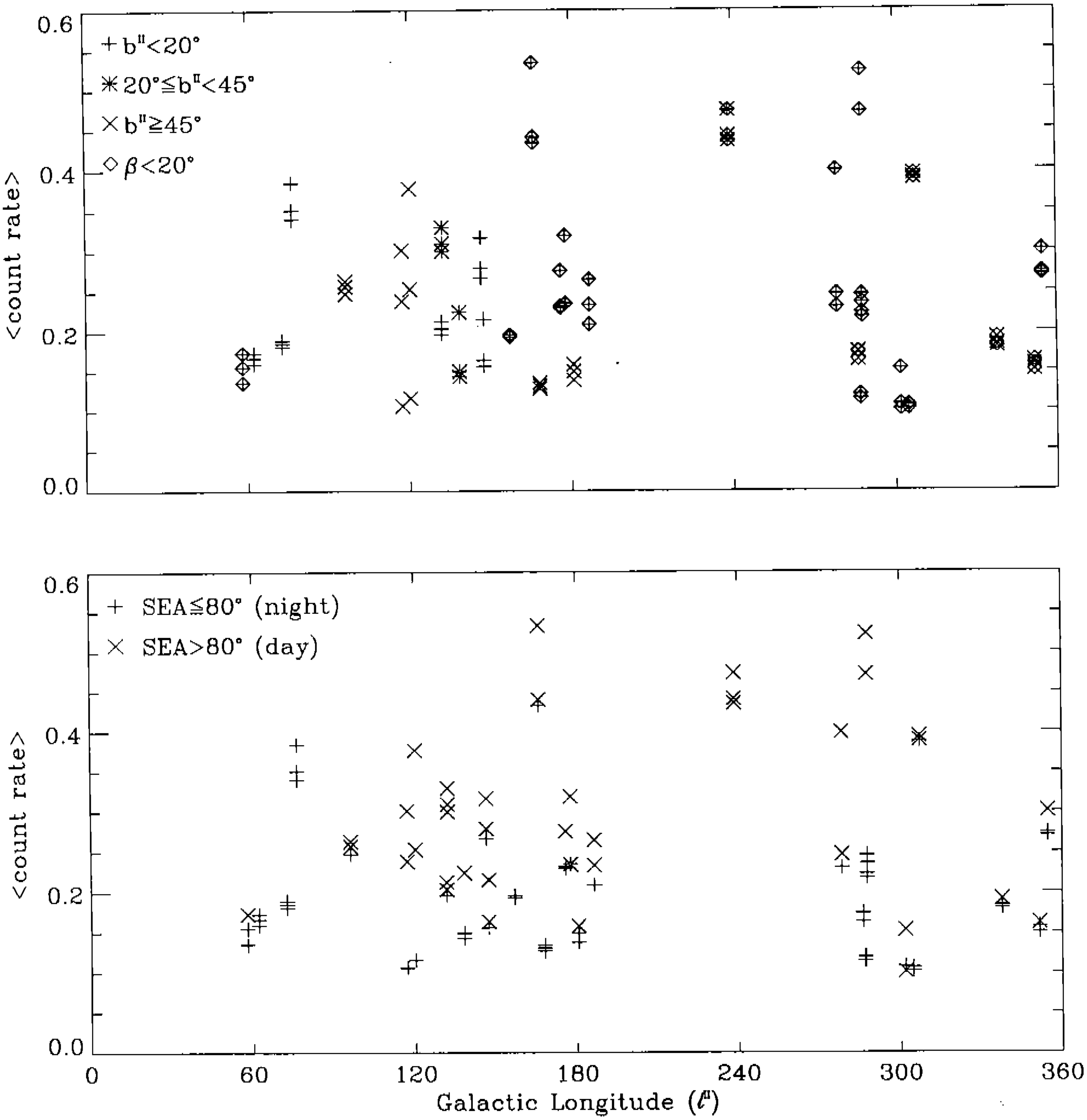

Figure 5: G650L Sky Count Rate as Diffuse Galactic Background.

The average count rate at the peak of the sky spectrum taken with the G650L disperser and the Red Digicon is plotted against the galactic longitude. In the top figure the data are further separated by galactic latitude. The correlation between count rate and the time of day aboard the spacecraft is shown in the bottom diagram.

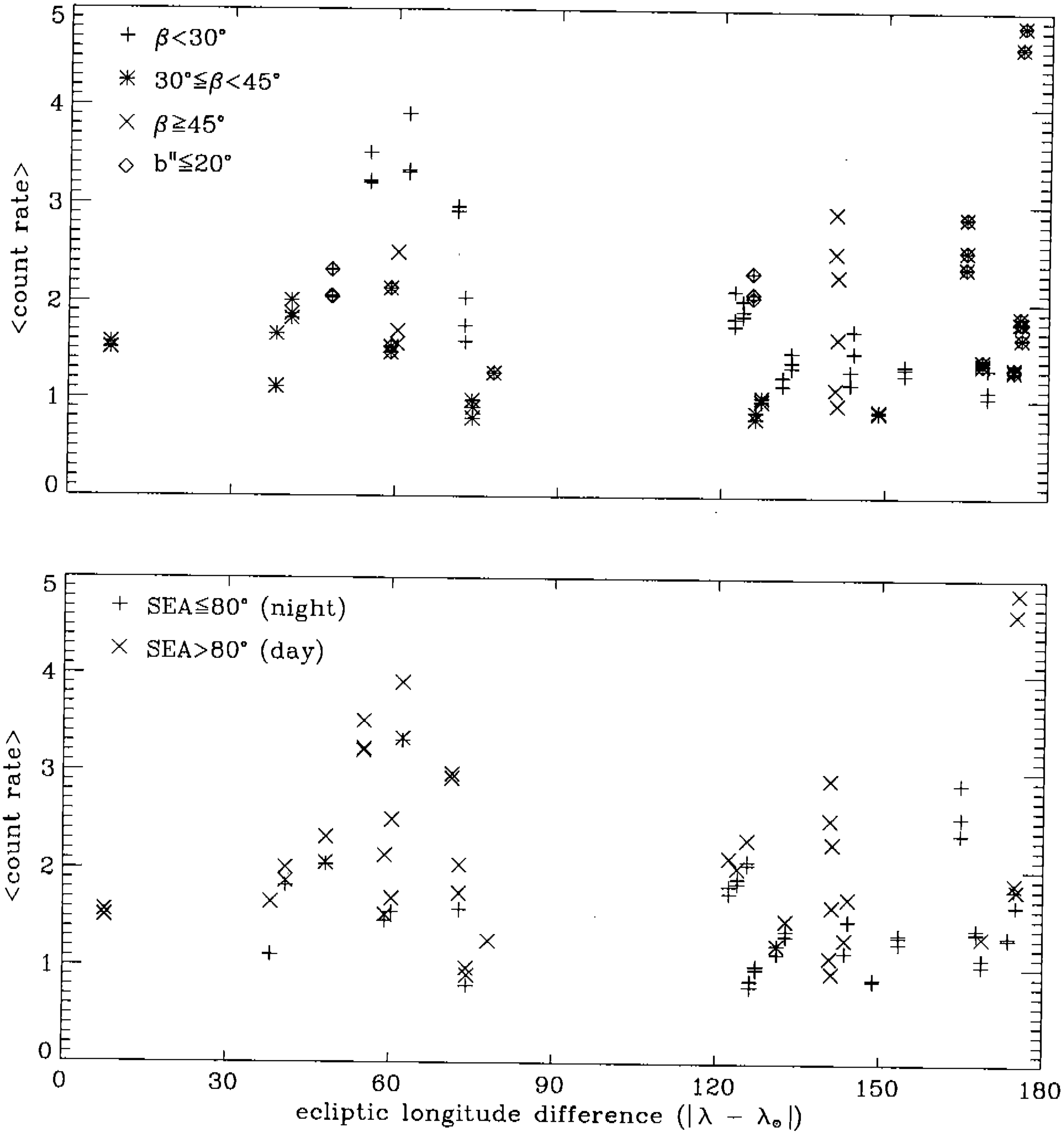

Figure 6: Relationship Between Prism Sky Count Rate and Zodiacal Light.

The average count rate at the peak of the sky spectrum taken with the prism disperser and the Red Digicon is plotted against the difference in ecliptic longitude (λ) between the sun and the target. In the top figure different symbols are used to designate different ecliptic latitudes (β). The correlation between count rate and the time of day aboard the spacecraft is shown in the bottom diagram.

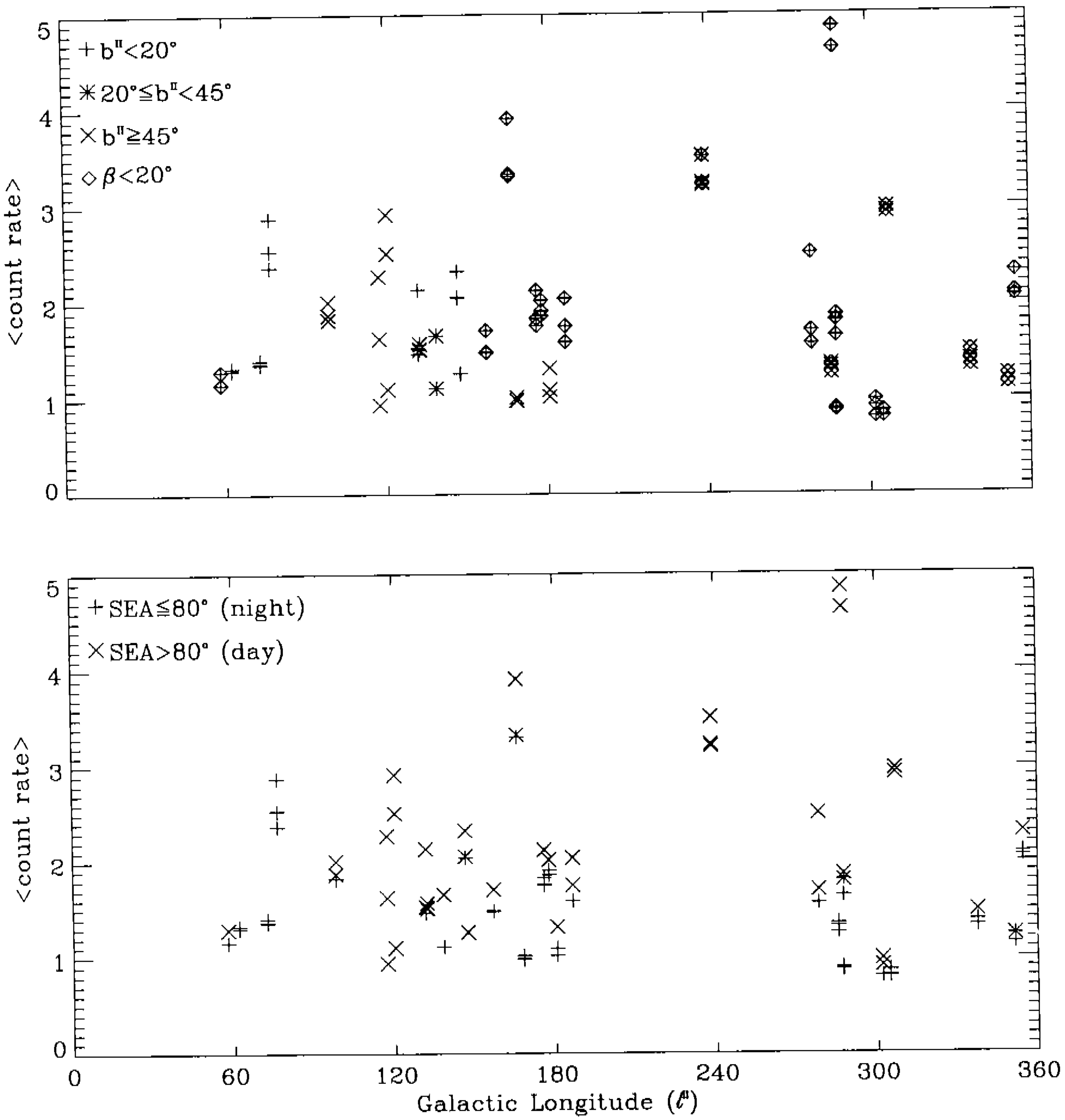

Figure 7: Prism Sky Count as Diffuse Galactic Background.

The average count rate at the peak of the sky spectrum taken with the prism disperser and the Red Digicon is plotted against the galactic longitude (ℓ^{II}). In the top figure the data are further separated by galactic latitude (b^{II}). The correlation between count rate and the time of day aboard the spacecraft is shown in the bottom diagram.

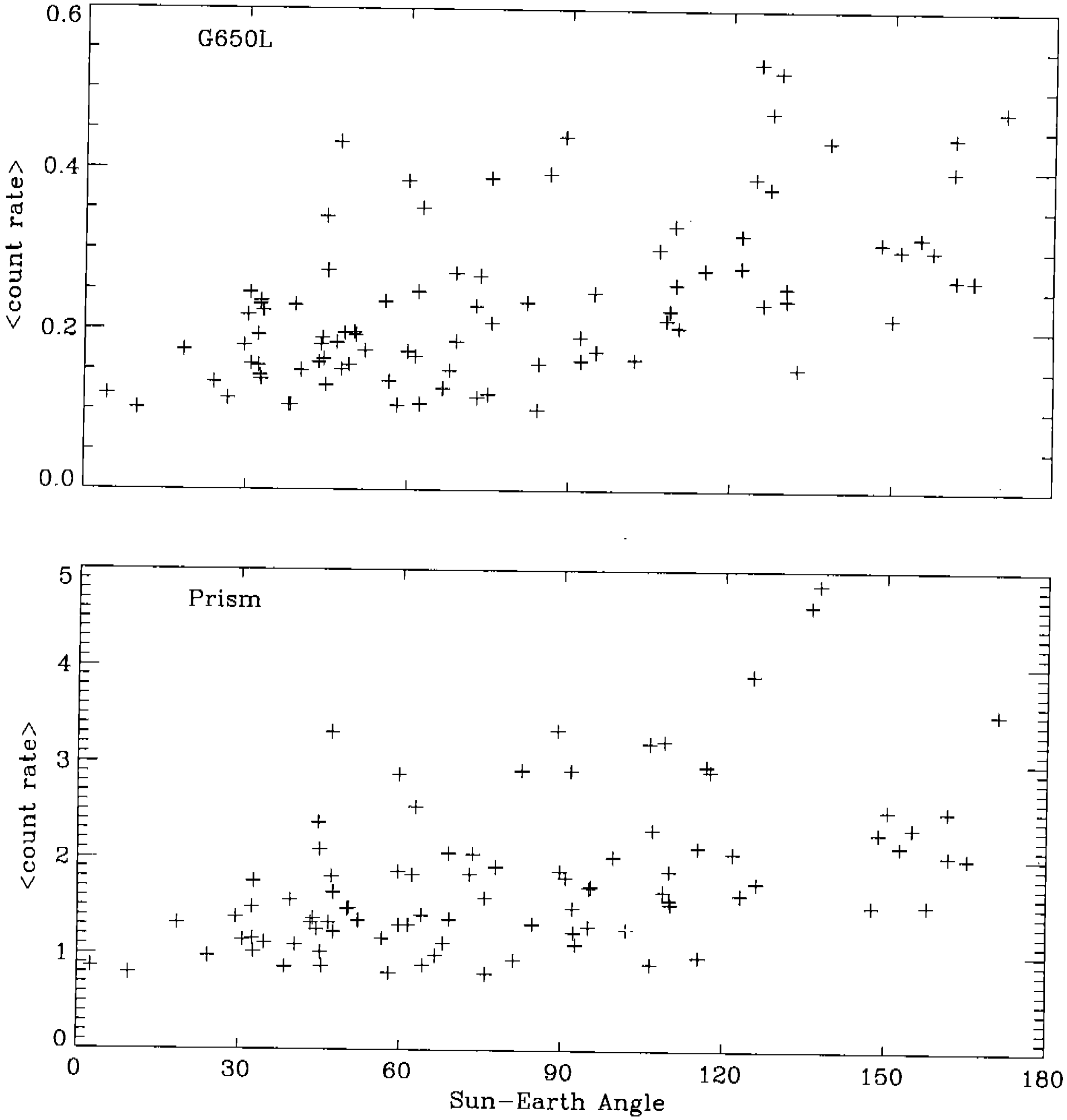

Figure 8: G650L and Prism Sky Count and Sun–Earth Angle.

The average count rate at the peak of the sky spectrum taken with the G650L and the prism is plotted against the sun–earth angle.

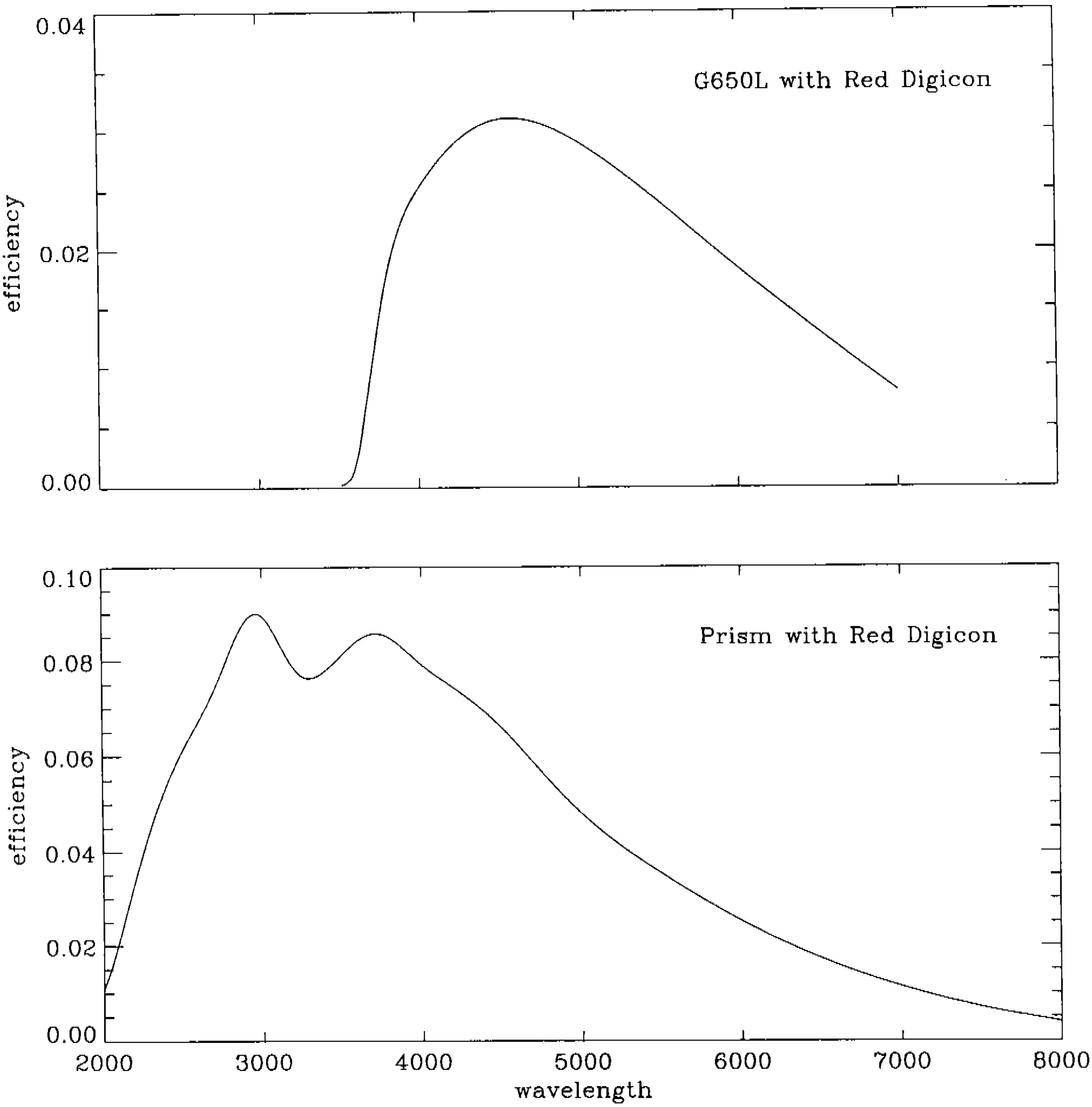

Figure 9: Efficiency Curves for G650L and Prism with Red Digicon.

The curves shown above were derived from data supplied by Don Neill (priv. comm.) and scaled to have the same peak count rates as those shown in the FOS Handbook (Kinney 1992). These curves were combined with the formulae in Table II to generate Figures 10 and 11.

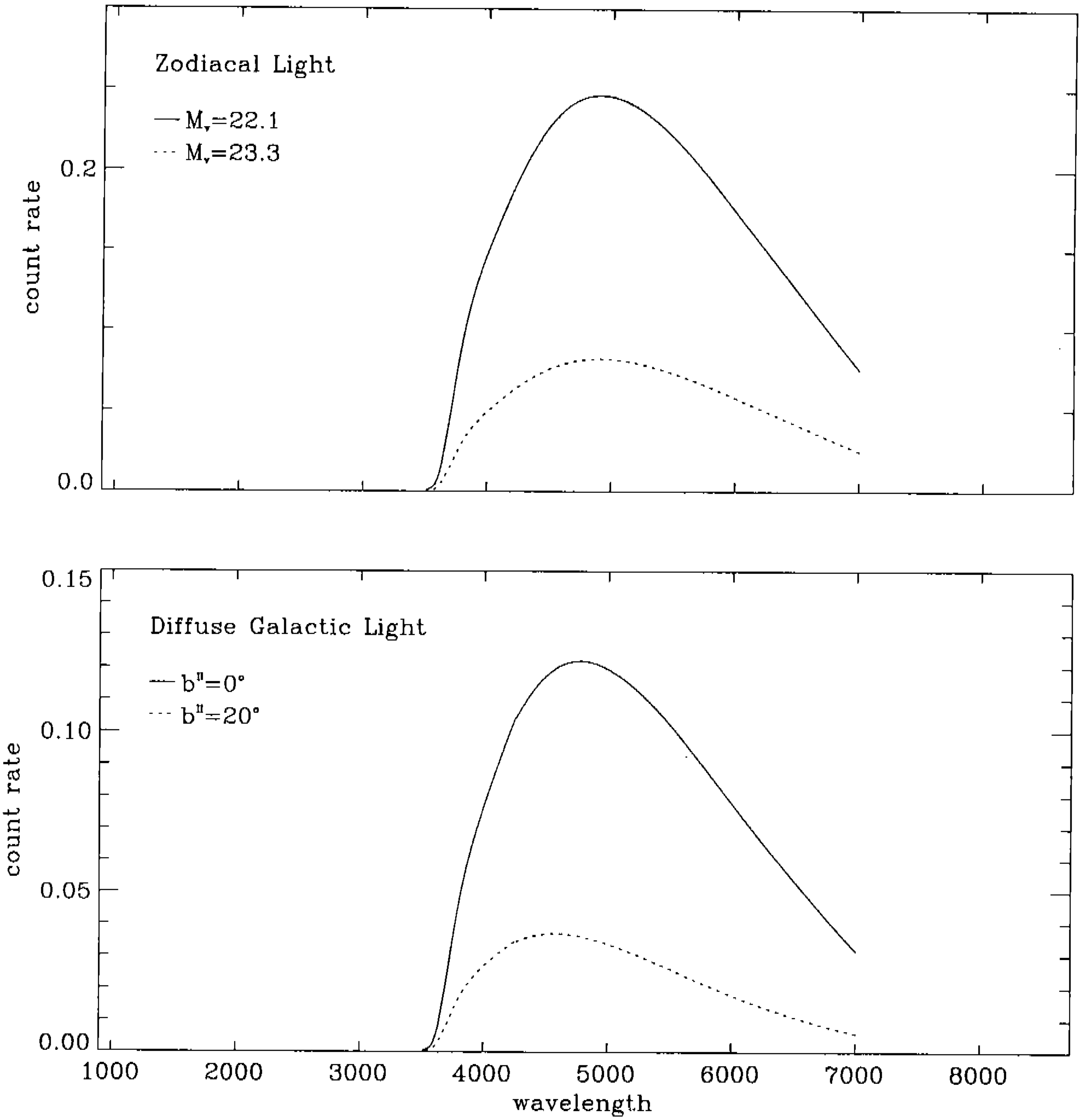

Figure 10: Predicted Sky Count Rates for G650L with Red Digicon.

The plots above were produced for the G650L grating and the Red Digicon based on the formula for the zodiacal light and the diffuse galactic background found in Table II.

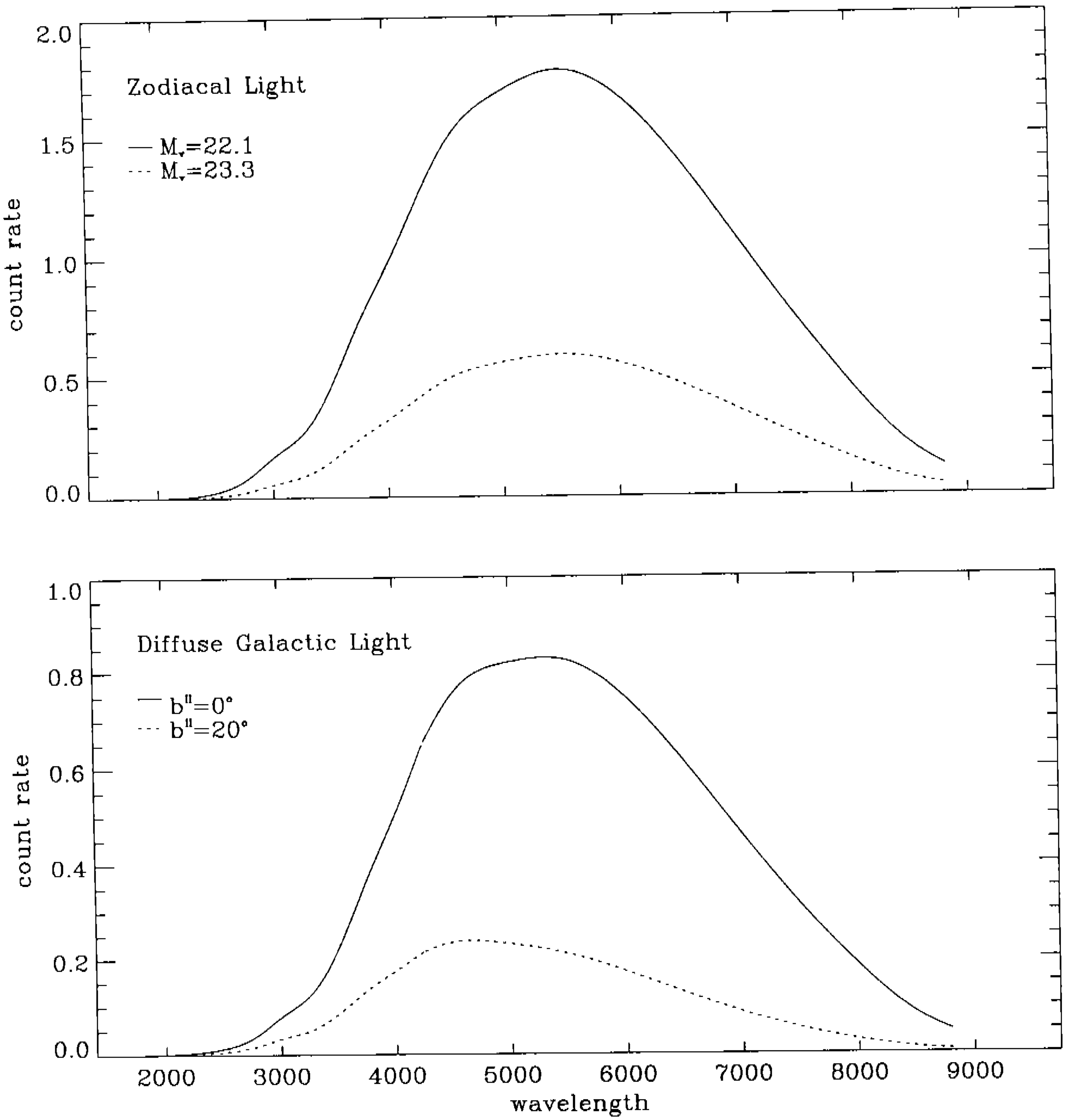

Figure 11: Predicted Sky Count Rates for the Prism and Red Digicon.

The plots above were produced for the prism disperser and the Red Digicon based on the formula for the zodiacal light and the diffuse galactic background found in Table II.

Appendix - Table I: Sky Background Count Rates for G160L + Blue Digicon.

File Name	SEA	ETA	SA	100	0 order	800	Lyβ	O I	Spectrum	Lyα	array
Y0G10201T	116	140	57	0.0113	0.8430	0.0114	1.1474	0.1596	0.0118	0.5795	53.107
Y0G10202T	91	116	57	0.0074	0.8415	0.0099	0.9267	0.0644	0.0105	0.4922	32.040
	108	133	57	0.0093	0.8426	0.0074	1.0785	0.1215	0.0100	0.5238	35.217
Y0G10203T	91	116	58	0.0082	0.8211	0.0061	0.9604	0.0641	0.0092	0.4985	32.122
	108	133	58	0.0076	0.8289	0.0084	1.1093	0.1330	0.0077	0.5622	35.543
	124	147	58	0.0085	0.8230	0.0076	1.1533	0.1800	0.0099	0.5775	37.413
Y0G10301T	122	144	88	0.0076	0.3604	0.0084	1.2300	0.2252	0.0086	0.6202	33.286
Y0G10302T	129	135	88	0.0097	0.4633	0.0091	1.2748	0.3089	0.0108	0.6850	37.050
	126	122	88	0.0088	0.5189	0.0086	1.3119	0.3282	0.0111	0.6633	38.770
Y0G10303T	90	114	88	0.0056	0.3430	0.0075	0.9981	0.0607	0.0062	0.5064	26.181
	102	128	88	0.0060	0.3707	0.0064	1.1548	0.1070	0.0077	0.5738	29.769
	114	139	88	0.0070	0.3352	0.0071	1.1585	0.1896	0.0083	0.5987	31.373
Y0G10401T	122	154	79	0.0068	0.3578	0.0065	1.2748	0.1941	0.0081	0.6539	33.177
Y0G10402T	89	117	79	0.0049	0.3707	0.0067	1.0567	0.0615	0.0060	0.5326	27.307
	101	134	79	0.0062	0.3696	0.0050	1.1596	0.0963	0.0071	0.5681	29.534
Y0G10403T	120	153	79	0.0077	0.3626	0.0077	1.2470	0.1978	0.0082	0.6053	32.605
	127	151	79	0.0078	0.3763	0.0086	1.2704	0.2204	0.0115	0.6496	34.823
	129	139	79	0.0089	0.4430	0.0089	1.3207	0.2878	0.0099	0.6431	36.640
Y0G10601T	150	133	73	0.0078	0.4207	0.0093	1.3530	0.2978	0.0078	0.6605	36.257
Y0G10602T	115	109	73	0.0067	0.4970	0.0064	1.2341	0.1741	0.0076	0.6575	34.417
	131	120	73	0.0054	0.4574	0.0069	1.3233	0.2256	0.0081	0.6946	36.320
Y0G10603T	149	132	73	0.0069	0.4170	0.0074	1.3311	0.2904	0.0091	0.6667	36.207
	148	132	73	0.0087	0.4185	0.0055	1.2856	0.3159	0.0074	0.6490	35.887
	138	126	73	0.0076	0.4504	0.0082	1.2944	0.2915	0.0112	0.6443	36.137
Y0G10701T	105	155	51	0.0102	0.7119	0.0093	1.1385	0.0944	0.0104	0.5767	35.563
Y0G10702T	129	157	51	0.0101	0.7348	0.0116	1.3200	0.3026	0.0127	0.6380	41.447
	139	142	51	0.0075	0.7744	0.0075	1.3352	0.4222	0.0087	0.6649	42.747
Y0G10703T	122	161	51	0.0100	0.7078	0.0127	1.2615	0.2452	0.0135	0.6054	39.567
	135	151	51	0.0107	0.7233	0.0090	1.3526	0.3656	0.0086	0.6920	42.080
	143	134	51	0.0095	0.8274	0.0079	1.4852	0.4722	0.0094	0.7172	46.073
Y0G10E01T	162	92	74	0.0062	1.1963	0.0056	1.9559	0.5770	0.0071	1.0029	60.543
Y0G10E02T	164	113	74	0.0077	0.5781	0.0054	1.5763	0.5278	0.0083	0.7419	44.643
	145	123	74	0.0076	0.5152	0.0086	1.3259	0.4585	0.0092	0.6602	39.583
Y0G10E03T	111	131	74	0.0107	0.4100	0.0103	0.9911	0.2448	0.0116	0.5160	31.685
	92	128	74	0.0107	0.3556	0.0097	0.8396	0.0748	0.0104	0.4037	25.326
	72	120	74	0.0095	0.3215	0.0099	0.6826	0.0241	0.0108	0.3594	21.082
Y0G10F01T	48	92	55	0.0102	0.3907	0.0081	0.5304	0.0115	0.0093	0.2828	18.565
Y0G10F02T	120	105	55	0.0055	0.7285	0.0090	1.5267	0.4044	0.0081	0.7753	44.983
	110	113	55	0.0058	0.5622	0.0069	1.2770	0.2478	0.0066	0.6373	36.410
Y0G10F03T	85	120	55	0.0061	0.4559	0.0061	0.9493	0.0522	0.0075	0.4811	26.326
	70	118	55	0.0060	0.4544	0.0076	0.8215	0.0137	0.0083	0.3974	23.387
	60	114	55	0.0079	0.4033	0.0080	0.6944	0.0126	0.0087	0.3501	21.463
Y0G10G01T	58	111	64	0.0063	1.9392	0.0063	0.5915	0.0115	0.0072	0.3207	48.127
Y0G10G02T	50	114	64	0.0054	1.8959	0.0072	0.4937	0.0196	0.0075	0.2519	46.047
	51	112	64	0.0068	1.9144	0.0065	0.4867	0.0093	0.0071	0.2249	46.803
Y0G10G03T	72	105	64	0.0082	2.2989	0.0086	0.7900	0.0252	0.0088	0.4081	56.490
	60	110	64	0.0064	2.2171	0.0078	0.5963	0.0159	0.0099	0.3168	50.113
	53	113	64	0.0076	2.2333	0.0061	0.5259	0.0096	0.0093	0.2571	48.530
Y0G10I01T	108	134	62	0.0060	0.5589	0.0062	1.0241	0.2104	0.0064	0.5173	31.199
Y0G10I02T	85	139	62	0.0064	0.4574	0.0060	0.8389	0.0485	0.0072	0.4285	24.659
	70	131	62	0.0053	0.4663	0.0078	0.7289	0.0115	0.0068	0.3476	21.789
Y0G10I03T	125	113	62	0.0079	0.6974	0.0079	1.4170	0.4270	0.0110	0.6990	43.367
	116	127	62	0.0070	0.5726	0.0076	1.1770	0.2970	0.0074	0.5886	35.053
	104	137	62	0.0067	0.5200	0.0079	1.0122	0.1693	0.0070	0.5105	30.164
Y0G10J01T	123	158	57	0.0080	0.8478	0.0085	1.0989	0.2233	0.0108	0.5486	37.570
Y0G10J02T	85	136	57	0.0093	0.8044	0.0067	0.8844	0.0478	0.0085	0.4669	30.678
	65	119	57	0.0079	0.7767	0.0078	0.7396	0.0163	0.0086	0.3667	26.949
Y0G10J03T	169	118	57	0.0080	1.0156	0.0086	1.6811	0.4567	0.0080	0.8304	52.087
	161	136	57	0.0089	0.9493	0.0075	1.4252	0.4270	0.0090	0.7190	46.700
	142	151	57	0.0074	0.8774	0.0063	1.2493	0.3422	0.0073	0.6429	41.317
Y0G10K01T	78	98	149	0.0082	0.8356	0.0079	0.7767	0.0833	0.0094	0.3956	29.618
Y0G10K02T	49	130	149	0.0080	0.3007	0.0073	0.2930	[illegible]	0.0058	0.1418	12.431

File Name	SEA	ETA	SA	100	0 order	800	Lyα	O I	Spectrum	Lyα	array
	33	148	149	0.0076	0.2985	0.0083	0.2226	0.0107	0.0082	0.1269	11.780
YOG10K03T	20	164	149	0.0072	0.3000	0.0076	0.1852	0.0078	0.0104	0.0923	11.270
	31	150	149	0.0078	0.2807	0.0072	0.2200	0.0052	0.0056	0.1231	10.546
	49	130	149	0.0053	0.3204	0.0054	0.2585	0.0081	0.0076	0.1281	11.366
YOG10L01T	30	117	144	0.0113	0.2974	0.0102	0.1941	0.0100	0.0117	0.0960	12.359
YOG10L02T	51	109	144	0.0070	0.2893	0.0061	0.2374	0.0122	0.0102	0.1444	12.701
	67	101	144	0.0071	0.4478	0.0060	0.5007	0.0178	0.0092	0.2617	19.098
YOG10L03T	28	117	144	0.0112	0.2885	0.0099	0.1844	0.0174	0.0146	0.0895	12.925
	38	114	144	0.0082	0.2770	0.0080	0.2085	0.0063	0.0102	0.1074	11.605
	53	108	144	0.0061	0.3093	0.0068	0.2741	0.0122	0.0072	0.1436	12.151
YOG10M01T	23	98	120	0.0054	0.2481	0.0077	0.1867	0.0078	0.0078	0.1006	10.013
YOG10M02T	138	94	120	0.0068	0.9819	0.0077	1.5030	0.5218	0.0096	0.7639	51.373
	118	111	120	0.0094	0.5400	0.0067	1.1259	0.2922	0.0103	0.5642	34.637
YOG10M03T	84	138	120	0.0071	0.3089	0.0074	0.6344	0.0344	0.0082	0.3212	19.254
	65	149	120	0.0054	0.2933	0.0060	0.4411	0.0119	0.0084	0.2233	14.852
	43	150	120	0.0069	0.2456	0.0068	0.2941	0.0126	0.0097	0.1546	12.064
YOG10N01T	47	97	149	0.0054	0.3537	0.0053	0.2552	0.0096	0.0062	0.1299	12.009
YOG10N02T	22	128	149	0.0073	0.3507	0.0051	0.2170	0.0141	0.0049	0.1118	10.944
	19	146	149	0.0049	0.3196	0.0056	0.2096	0.0063	0.0059	0.1136	10.491
YOG10N03T	44	160	149	0.0080	0.3352	0.0071	0.2948	0.0085	0.0080	0.1532	13.086
	62	147	149	0.0091	0.3633	0.0067	0.4600	0.0137	0.0084	0.2156	16.121
	80	129	149	0.0069	0.4130	0.0080	0.7815	0.0244	0.0077	0.3890	22.837
YOG10O01R	82	92	107	0.0064	0.6037	0.0055	0.9518	0.0852	0.0076	0.4541	28.558
YOG10O02R	110	97	107	0.0042	0.7241	0.0063	1.3604	0.4033	0.0092	0.7027	41.913
	126	99	107	0.0081	0.9859	0.0089	1.6741	0.9348	0.0103	0.8639	58.540
YOG10O03R	148	99	107	0.0097	1.0567	0.0081	1.5352	1.2196	0.0118	0.8258	61.217
	150	98	107	0.0103	1.2156	0.0091	1.4948	1.2070	0.0129	0.7818	62.023
	142	95	107	0.0103	1.2893	0.0123	1.4222	1.1430	0.0144	0.7950	62.627
YOG10P01T	102	148	96	0.0059	0.3370	0.0065	0.8489	0.1348	0.0083	0.4325	24.502
YOG10P02T	71	165	96	0.0092	0.2696	0.0072	0.6226	0.0181	0.0078	0.3223	18.767
	57	151	96	0.0091	0.2526	0.0091	0.4767	0.0107	0.0098	0.2343	16.280
YOG10P03T	125	120	96	0.0059	0.5385	0.0062	1.1722	0.3215	0.0080	0.6007	35.097
	110	139	96	0.0077	0.3396	0.0071	0.9378	0.1841	0.0069	0.4786	26.799
	92	159	96	0.0060	0.3130	0.0083	0.7748	0.0733	0.0085	0.3851	22.246
YOG10R01T	80	141	130	0.0067	0.3844	0.0089	0.6226	0.0215	0.0090	0.3170	20.271
YOG10R02T	50	148	130	0.0071	0.3533	0.0074	0.3015	0.0078	0.0055	0.1523	13.112
	35	139	130	0.0071	0.3544	0.0077	0.2041	0.0067	0.0070	0.1113	11.391
YOG10R03T	112	116	129	0.0113	0.5207	0.0153	0.9885	0.1856	0.0147	0.4953	32.777
	91	133	129	0.0087	0.4004	0.0085	0.7259	0.0641	0.0107	0.3720	23.077
	71	146	129	0.0081	0.3589	0.0080	0.4978	0.0107	0.0072	0.2409	17.072
YOG10S01T	82	149	126	0.0056	0.3659	0.0071	0.6367	0.0241	0.0079	0.3140	19.502
YOG10S02T	52	157	126	0.0052	0.3148	0.0073	0.3174	0.0085	0.0066	0.1605	12.937
	37	146	126	0.0074	0.3100	0.0080	0.2270	0.0052	0.0065	0.1194	11.192
YOG10S03T	113	119	126	0.0064	0.4459	0.0066	1.0230	0.1896	0.0080	0.4939	29.272
	93	139	126	0.0062	0.3400	0.0076	0.7359	0.0611	0.0086	0.3838	21.985
	73	155	126	0.0067	0.3148	0.0060	0.5441	0.0126	0.0077	0.2625	16.792
YOG10T01T	68	144	146	0.0068	0.3433	0.0098	0.5367	0.0126	0.0078	0.2838	17.524
YOG10T02T	49	151	146	0.0074	0.3019	0.0063	0.3311	0.0141	0.0101	0.1720	13.513
	42	142	146	0.0068	0.3126	0.0064	0.2482	0.0059	0.0074	0.1341	11.725
YOG10T03T	91	119	146	0.0071	0.3981	0.0071	0.8896	0.1037	0.0089	0.4753	26.077
	74	138	146	0.0063	0.3556	0.0065	0.6522	0.0230	0.0077	0.3371	20.055
	61	149	146	0.0074	0.3233	0.0081	0.4593	0.0115	0.0084	0.2321	16.326
YOG10U01T	66	150	142	0.0063	0.3452	0.0082	0.4422	0.0122	0.0089	0.2306	16.044
YOG10U02T	38	161	142	0.0060	0.3178	0.0068	0.2033	0.0074	0.0065	0.1170	10.786
	25	150	142	0.0082	0.3156	0.0064	0.1593	0.0100	0.0073	0.0901	10.165
YOG10U03T	93	122	142	0.0058	0.3904	0.0075	0.7756	0.0667	0.0079	0.3860	23.138
	73	143	142	0.0070	0.3426	0.0056	0.5070	0.0152	0.0137	0.2723	17.414
	55	158	142	0.0059	0.3211	0.0057	0.3341	0.0115	0.0105	0.1519	13.140
YOG10V01T	65	150	143	0.0071	0.3285	0.0092	0.4322	0.0167	0.0099	0.2304	16.061
YOG10V02T	38	161	143	0.0068	0.3089	0.0060	0.2152	0.0067	0.0068	0.1268	11.027
	25	149	143	0.0056	0.3374	0.0057	0.1763	0.0078	0.0054	0.0886	10.245
YOG10V03T	93	122	143	0.0065	0.3793	0.0076	0.7848	0.0652	0.0099	0.4135	23.566

File Name	SEA	ETA	SA	100	0 order	800	Lyα	O I	Spectrum	Lyα	array
	73	143	143	0.0065	0.3556	0.0062	0.5378	0.0163	0.0100	0.2741	17.601
	55	158	143	0.0058	0.3226	0.0069	0.3256	0.0081	0.0074	0.1584	13.112
Y0G10W01T	143	136	77	0.0069	0.3667	0.0082	1.0922	0.4430	0.0093	0.5674	33.807
Y0G10W02T	115	143	77	0.0080	0.3648	0.0100	0.8841	0.2618	0.0102	0.4356	28.014
	97	137	77	0.0081	0.3189	0.0092	0.8096	0.1474	0.0103	0.3853	24.342
Y0G10W03T	153	116	77	0.0053	0.4674	0.0069	1.3733	0.5226	0.0078	0.6908	39.993
	149	131	77	0.0076	0.3719	0.0087	1.1226	0.4837	0.0111	0.5888	35.527
	135	141	77	0.0078	0.3400	0.0088	1.0530	0.3996	0.0109	0.5357	32.376
Y0G10X01T	129	152	77	0.0084	0.3552	0.0084	0.9841	0.3985	0.0083	0.4889	30.949
Y0G10X02T	101	163	77	0.0085	0.2904	0.0091	0.7885	0.1911	0.0114	0.3968	24.678
	83	150	77	0.0085	0.2567	0.0071	0.7052	0.0500	0.0095	0.3492	20.446
Y0G10X03T	149	125	77	0.0073	0.4833	0.0061	1.2289	0.4796	0.0080	0.6412	37.990
	137	143	77	0.0073	0.3641	0.0062	1.0848	0.4348	0.0079	0.5175	32.179
	121	159	77	0.0092	0.3204	0.0090	0.8770	0.3326	0.0105	0.4812	28.814
Y0G10Y01T	23	97	83	0.0062	0.1907	0.0073	0.2989	0.0115	0.0085	0.1360	78.627
Y0G10Y02T	53	105	83	0.0062	0.2059	0.0053	0.4744	0.0122	0.0070	0.2624	588.157
	73	107	83	0.0052	0.2267	0.0064	0.7685	0.0189	0.0083	0.3968	20.398
Y0G10Y03T	106	107	83	0.0056	0.4193	0.0066	1.3230	0.2244	0.0084	0.7015	35.800
	125	103	83	0.0071	0.5619	0.0064	1.5522	0.4093	0.0092	0.7694	43.780
	144	99	83	0.0061	0.7326	0.0073	1.7778	0.6389	0.0080	0.9124	156.470
Y0G11001T	34	138	141	0.0071	0.3078	0.0054	0.1841	0.0085	0.0081	0.0894	10.231
Y0G11002T	48	155	141	0.0100	0.3178	0.0083	0.2444	0.0056	0.0114	0.1362	13.454
	61	150	141	0.0137	0.3278	0.0123	0.3482	0.0141	0.0132	0.1765	16.459
Y0G11003T	38	114	141	0.0049	0.2989	0.0048	0.1748	0.0056	0.0056	0.0858	35.623
	33	131	141	0.0053	0.3037	0.0053	0.1693	0.0096	0.0065	0.0995	11.017
	37	146	141	0.0079	0.3252	0.0060	0.1904	0.0089	0.0078	0.0936	10.625
Y0G11101T	43	156	126	0.0084	0.3122	0.0077	0.3115	0.0074	0.0109	0.1589	15.095
Y0G11102T	75	144	126	0.0062	0.3500	0.0067	0.6593	0.0137	0.0090	0.3482	20.393
	94	128	126	0.0061	0.4026	0.0083	1.0385	0.0670	0.0092	0.5227	32.287
Y0G11104T	61	153	126	0.0096	0.3352	0.0085	0.4426	0.0096	0.0071	0.2682	17.599
Y0G11105T	93	129	126	0.0103	0.3978	0.0072	0.9922	0.0626	0.0073	0.5237	29.013
	113	112	126	0.0109	0.5422	0.0096	1.4500	0.1726	0.0116	0.7152	39.793
Y0G11106T	12	115	126	0.0132	0.3263	0.0107	0.1948	0.0174	0.0117	0.1073	13.238
	9	132	126	0.0126	0.3226	0.0103	0.2056	0.0115	0.0126	0.1099	13.301
	23	147	126	0.0135	0.3244	0.0107	0.2233	0.0107	0.0099	0.1125	13.652
Y0G11201T	34	105	137	0.0063	0.2656	0.0048	0.1637	0.0059	0.0050	0.0875	8.931
Y0G11202T	42	110	137	0.0044	0.2478	0.0055	0.1878	0.0059	0.0057	0.1089	9.039
	54	110	137	0.0077	0.2737	0.0086	0.2600	0.0070	0.0080	0.1453	11.984
Y0G11203T	80	104	137	0.0105	0.3211	0.0105	0.5970	0.0267	0.0115	0.3238	20.539
	95	98	137	0.0130	0.3996	0.0095	0.8963	0.0807	0.0109	0.4497	27.030
	111	92	137	0.0090	0.7530	0.0105	1.2570	0.1789	0.0123	0.6301	39.313
Y0G11301T	8	151	144	0.0078	0.2670	0.0074	0.1433	0.0093	0.0057	0.0673	9.191
Y0G11302T	36	115	144	0.0055	0.2526	0.0049	0.1748	0.0074	0.0053	0.0875	8.748
	17	132	144	0.0065	0.2500	0.0075	0.1515	0.0104	0.0062	0.0767	9.162
Y0G11303T	14	157	144	0.0085	0.2530	0.0072	0.1511	0.0074	0.0081	0.0794	9.698
	31	156	144	0.0084	0.2626	0.0069	0.1807	0.0107	0.0073	0.0884	10.022
	51	145	144	0.0087	0.2711	0.0078	0.2426	0.0100	0.0073	0.1444	11.862
Y0G11501T	32	141	146	0.0062	0.2811	0.0067	0.2174	0.0107	0.0063	0.1076	10.587
Y0G11502T	33	127	146	0.0061	0.2700	0.0075	0.2085	0.0074	0.0079	0.1046	10.576
	52	111	146	0.0063	0.2789	0.0096	0.2867	0.0104	0.0087	0.1589	12.931
Y0G11503T	61	121	146	0.0096	0.2881	0.0078	0.4119	0.0148	0.0089	0.2165	15.600
	41	135	146	0.0091	0.2841	0.0101	0.2622	0.0122	0.0099	0.1308	12.869
	22	146	146	0.0068	0.2830	0.0095	0.2041	0.0107	0.0075	0.1034	11.040
Y0G11601T	15	156	142	0.0146	0.2515	0.0134	0.1978	0.0115	0.0122	0.1045	13.253
Y0G11602T	33	143	142	0.0080	0.2700	0.0065	0.2607	0.0111	0.0086	0.1307	11.821
	51	127	142	0.0056	0.2648	0.0068	0.3422	0.0070	0.0067	0.1828	12.542
Y0G11603T	16	156	142	0.0093	0.2544	0.0105	0.2167	0.0115	0.0105	0.1070	12.028
	25	150	142	0.0087	0.2378	0.3091	0.2326	0.0093	0.0102	0.1178	11.532
	42	136	142	0.0078	0.2689	0.0091	0.2833	0.0115	0.0113	0.1597	13.171
Y0G20101T	67	132	66	0.0055	0.4289	0.0057	0.5915	0.0096	0.0075	0.3094	18.996
Y0G20102T	97	149	66	0.0062	0.4541	0.0065	0.9426	0.0663	0.0081	0.4634	26.780
	115	148	66	0.0057	0.4944	0.0060	1.1556	[illegible]	0.0100	0.5494	31.921

Appe - Table I: Sky Background Count Rates for G160L + Blue con.

File Name	SEA	ETA	SA	100	0 order	800	Lyα	O I	Spectrum	Lyα	array
YOG20103T	41	108	66	0.0063	0.3922	0.0057	0.3533	0.0104	0.0079	0.1809	14.537
	58	124	66	0.0056	0.4070	0.0064	0.5289	0.0119	0.0081	0.2651	17.762
	76	139	66	0.0062	0.4589	0.0077	0.7363	0.0159	0.0082	0.3568	22.401
YOG20301T	60	146	92	0.0068	0.3900	0.0069	0.4818	0.0119	0.0099	0.2371	17.043
YOG20302T	93	154	92	0.0076	0.4367	0.0090	0.8193	0.0874	0.0111	0.4107	25.865
	112	145	92	0.0072	0.4767	0.0080	1.0248	0.1737	0.0108	0.5216	30.854
YOG20303T	33	123	92	0.0066	0.3722	0.0075	0.2789	0.0067	0.0062	0.1484	13.130
	52	140	92	0.0057	0.3759	0.0063	0.3763	0.0085	0.0083	0.2052	14.842
	71	152	92	0.0071	0.4011	0.0094	0.6033	0.0167	0.0105	0.3232	20.364
YOG20701T	55	135	84	0.0064	0.3530	0.0068	0.4237	0.0089	0.0080	0.2103	15.170
YOG20702T	84	145	84	0.0060	0.4030	0.0069	0.7274	0.0293	0.0074	0.3824	21.795
	102	140	84	0.0062	0.4189	0.0077	1.0404	0.0948	0.0090	0.5078	28.116
YOG20703T	26	107	84	0.0062	0.3330	0.0060	0.2448	0.0074	0.0071	0.1268	11.816
	39	123	84	0.0051	0.3437	0.0048	0.2878	0.0048	0.0064	0.1585	12.259
	55	136	84	0.0070	0.3056	0.0063	0.4318	0.0096	0.0078	0.2119	15.189
YOG20D01T	45	128	84	0.0071	0.6889	0.0071	0.3233	0.0100	0.0078	0.1801	18.114
YOG20D02T	70	145	84	0.0061	0.7144	0.0066	0.5626	0.0163	0.0077	0.2945	22.584
	86	145	84	0.0070	0.7656	0.0076	0.7678	0.0300	0.0074	0.3979	27.195
YOG20D03T	32	105	84	0.0058	0.6844	0.0054	0.2530	0.0085	0.0064	0.1353	15.836
	39	121	84	0.0043	0.7052	0.0045	0.2822	0.0074	0.0078	0.1454	16.507
	52	135	84	0.0056	0.6774	0.0057	0.3322	0.0107	0.0080	0.1901	18.129
YOG20F01T	142	104	91	0.0116	1.0985	0.0110	1.6219	0.4830	0.0138	0.8075	54.347
YOG20F02T	12	98	91	0.0074	0.6011	0.0071	0.1937	0.0081	0.0089	0.1097	15.130
	22	110	91	0.0059	0.5944	0.0057	0.2444	0.0085	0.0070	0.1007	14.745
YOG20F03T	92	128	91	0.0121	0.7030	0.0119	0.9274	0.0781	0.0184	0.4931	33.199
	111	121	91	0.0134	0.7822	0.0136	1.2148	0.1759	0.0167	0.6105	40.550
	131	112	91	0.0122	0.9663	0.0107	1.4537	0.3570	0.0180	0.7399	49.313
YOG20L01T	89	136	51	0.0098	1.3585	0.0120	1.0248	0.0648	0.0168	0.5137	42.243
YOG20L02T	121	158	51	0.0100	1.4004	0.0098	1.2378	0.2811	0.0167	0.6289	48.497
	141	156	51	0.0079	1.4623	0.0076	1.3526	0.4133	0.0144	0.6450	51.840
YOG20L03T	61	110	51	0.0077	1.3063	0.0069	0.7589	0.0163	0.0118	0.3756	33.740
	80	128	51	0.0096	1.3808	0.0095	0.9878	0.0315	0.0154	0.4803	40.587
	100	145	51	0.0116	1.3867	0.0137	1.1022	0.1315	0.0190	0.5877	45.830
YOG20N01T	165	91	83	0.0047	1.3523	0.0064	1.8459	0.6022	0.0122	0.9695	62.320
YOG20N02T	159	113	83	0.0068	0.6422	0.0063	1.3974	0.5011	0.0106	0.7261	43.000
	140	124	83	0.0094	0.5322	0.0096	1.1933	0.4026	0.0102	0.6107	38.067
YOG20N03T	106	133	83	0.0114	0.4648	0.0112	0.8859	0.1641	0.0161	0.4662	29.663
	86	131	83	0.0136	0.3996	0.0143	0.7319	0.0444	0.0155	0.3816	25.568
	67	123	83	0.0145	0.3848	0.0135	0.5304	0.0174	0.0192	0.2702	21.666
YOG20P01T	139	113	58	0.0073	0.8470	0.0079	1.6333	0.4815	0.0164	0.8418	50.657
YOG20P02T	169	119	58	0.0081	0.8226	0.0075	1.5648	0.6693	0.0140	0.8176	51.723
	168	118	58	0.0057	0.8130	0.0082	1.5896	0.6856	0.0132	0.7714	51.357
YOG20P03T	110	102	58	0.0062	0.8659	0.0063	1.6070	0.2752	0.0127	0.7781	46.627
	130	110	58	0.0076	0.8970	0.3069	1.6515	0.4130	0.0132	0.8174	50.150
	149	116	58	0.0078	0.8452	0.0090	1.6019	0.5411	0.0130	0.8423	51.363
YOG20T01T	163	122	69	0.0065	0.6996	0.0075	1.4144	0.5007	0.0112	0.7018	44.140
YOG20T02T	144	127	69	0.0079	0.7063	0.0097	1.2804	0.5000	0.0131	0.6169	42.053
	123	122	69	0.0106	0.7000	0.0095	1.1563	0.3918	0.0162	0.6066	40.133
YOG20T03T	145	108	69	0.0086	0.8356	0.0078	1.6333	0.3974	0.0114	0.8207	48.820
	160	119	69	0.0082	0.7393	0.0083	1.4996	0.4956	0.0112	0.7508	46.377
	161	126	69	0.0075	0.6722	0.0081	1.3985	0.4996	0.0116	0.6881	43.883
YOG20V01T	41	86	114	0.0071	0.5878	0.0054	0.2459	0.0230	0.0114	0.1220	16.024
YOG20V02T	16	99	114	0.0073	0.5589	0.0062	0.1833	0.0093	0.0106	0.1133	14.619
	19	104	114	0.0073	0.5156	0.0071	0.1885	0.0130	0.0105	0.1083	14.314
YOG20V03T	48	109	114	0.0062	0.5378	0.0068	0.2630	0.0093	0.0117	0.1558	15.591
	67	109	114	0.0063	0.5796	0.0068	0.4467	0.0104	0.0115	0.2270	19.319
	86	106	114	0.0093	0.8019	0.0085	0.7500	0.0396	0.0122	0.3872	28.633
YOG20X01T	38	88	114	0.0070	0.6167	0.0080	0.2367	0.0330	0.0114	0.1223	16.257
YOG20X02T	15	100	114	0.0066	0.5681	0.0060	0.1789	0.0181	0.0095	0.1067	14.220
	20	105	114	0.0067	0.5852	0.0060	0.1974	0.0100	0.0099	0.1036	14.588
YOG20X03T	51	109	115	0.0066	0.6344	0.0049	0.2867	0.0059	0.0102	0.1586	16.726
	70	109	115	0.0086	0.8685	0.0091	0.5041	0.0100	0.0128	0.2544	23.876

File Name	SEA	ETA	SA	100	0 order	800	Lyα	O I	Spectrum	Lyα	array
	89	106	115	0.0109	1.0926	0.0077	0.8418	0.0648	0.0182	0.4167	37.260
Y0G21V01T	53	138	151	0.0069	0.3726	0.0077	0.3026	0.0152	0.0077	0.1734	13.977
Y0G21V02T	33	161	151	0.0066	0.3741	0.0055	0.2007	0.0070	0.0078	0.1045	11.596
	49	142	151	0.0063	0.3963	0.0066	0.2856	0.0044	0.0072	0.1299	13.156
Y0G21V03T	23	168	151	0.0074	0.3841	0.0087	0.1859	0.0078	0.0092	0.0819	11.925
	35	158	151	0.0089	0.3711	0.0067	0.2048	0.0111	0.0085	0.1077	26.106
	52	139	151	0.0071	0.3841	0.0073	0.3067	0.0074	0.0081	0.1411	35.910
Y0G21X01T	14	139	138	0.0071	0.3656	0.0056	0.2222	0.0085	0.0094	0.1091	22.139
Y0G21X02T	23	156	138	0.0067	0.3700	0.0054	0.2133	0.0085	0.0081	0.1121	18.597
	40	151	138	0.0072	0.3789	0.0060	0.2941	0.0111	0.0110	0.1546	69.693
Y0G21X03T	37	114	138	0.0111	0.3937	0.0126	0.2548	0.0152	0.0138	0.1226	15.733
	20	131	138	0.0092	0.3770	0.0085	0.2144	0.0093	0.0138	0.1132	13.833
	13	147	138	0.0074	0.3741	0.0060	0.2063	0.0100	0.0089	0.1096	11.923
Y0G22301T	37	93	78	0.0055	0.4256	0.0051	0.3944	0.0207	0.0095	0.2175	16.953
Y0G22302T	47	124	78	0.0069	0.4967	0.0081	0.4889	0.0141	0.0109	0.2477	19.976
	59	141	78	0.0047	0.4489	0.0062	0.5633	0.0081	0.0105	0.3024	19.554
Y0G22303T	85	160	78	0.0066	0.5159	0.0073	0.7700	0.0815	0.0097	0.3823	24.929
	100	154	78	0.0060	0.5400	0.0063	0.9544	0.2189	0.0089	0.4646	29.506
	115	138	78	0.0071	0.6233	0.0085	1.0559	0.3882	0.0111	0.5515	35.827
Y0G22701T	150	90	72	0.0082	1.2819	0.0105	1.6467	0.5826	0.0139	0.8522	64.967
Y0G22702T	35	82	72	0.0078	0.3881	0.0065	0.2685	0.0296	0.0095	0.1535	13.949
	26	92	72	0.0076	0.3833	0.0055	0.2459	0.0137	0.0084	0.1203	12.670
Y0G22703T	96	119	72	0.0108	0.4926	0.0129	0.8959	0.1044	0.0199	0.4584	31.116
	113	113	72	0.0156	0.5848	0.0129	1.1048	0.2211	0.0175	0.5966	37.377
	130	104	72	0.0142	0.7222	0.0155	1.3285	0.3500	0.0190	0.6771	45.407
Y0G22901T	51	103	62	0.0056	0.4826	0.0065	0.5137	0.0070	0.0066	0.2626	31.649
Y0G22902T	76	101	62	0.0069	0.6585	0.0074	0.9118	0.0378	0.0085	0.4453	39.840
	92	98	62	0.0096	0.8415	0.0089	1.2552	0.1289	0.0122	0.6536	54.673
Y0G22903T	79	83	62	0.0114	0.9811	0.0097	1.0207	0.0622	0.0172	0.5958	42.577
	64	87	62	0.0112	0.5070	0.0107	0.6781	0.0244	0.0151	0.3419	27.230
	49	91	62	0.0084	0.4874	0.0111	0.4926	0.0259	0.0181	0.2581	25.902
Y0G30101T	31	113	124	0.0105	0.3893	0.0110	0.1870	0.0144	0.0146	0.1022	14.128
Y0G30102T	53	125	124	0.0149	0.4444	0.0141	0.3204	0.0174	0.0137	0.1743	18.191
	70	127	124	0.0144	0.4733	0.0129	0.4985	0.0178	0.0188	0.2770	22.249
Y0G30103T	54	125	124	0.0142	0.4452	0.0112	0.3126	0.0181	0.0150	0.1664	17.649
	71	127	124	0.0186	0.4581	0.0150	0.5078	0.0196	0.0138	0.2815	22.824
	88	124	124	0.0084	0.4830	0.0085	0.8093	0.0559	0.0120	0.3969	25.707
Y0G30301T	52	140	95	0.0090	0.5733	0.0118	0.3630	0.0167	0.0113	0.1890	19.023
Y0G30302T	80	168	95	0.0124	0.6037	0.0128	0.6700	0.0285	0.0165	0.3509	26.409
	97	165	95	0.0104	0.6433	0.0097	0.9030	0.0785	0.0111	0.4459	29.949
Y0G30303T	32	111	95	0.0053	0.5848	0.0057	0.2278	0.0052	0.0070	0.1329	14.009
	44	130	95	0.0076	0.5393	0.0073	0.3096	0.0100	0.0083	0.1640	16.083
	60	150	95	0.0082	0.5659	0.0107	0.4356	0.0093	0.0116	0.2442	19.883
Y0G30501T	54	140	93	0.0077	0.5896	0.0057	0.3448	0.0104	0.0080	0.1733	17.274
Y0G30502T	81	170	93	0.0065	0.6526	0.0074	0.6941	0.0248	0.0090	0.3139	23.859
	98	167	93	0.0078	0.6607	0.0077	0.8715	0.0670	0.0083	0.4281	28.210
Y0G30503T	34	111	93	0.0045	0.5959	0.0053	0.2322	0.0089	0.0063	0.1220	14.194
	46	131	93	0.0064	0.5944	0.0068	0.2900	0.0078	0.0066	0.1527	15.618
	62	150	93	0.0093	0.5759	0.0078	0.4415	0.0081	0.0092	0.2164	19.459
Y0G30701T	98	142	50	0.0065	1.4829	0.0069	1.1852	0.0581	0.0077	0.5811	43.410
Y0G30702T	59	104	50	0.0049	1.4456	0.0046	0.6322	0.0122	0.0071	0.3194	31.958
	70	119	50	0.0074	1.4589	0.0044	0.7807	0.0133	0.0071	0.3989	35.463
Y0G30703T	92	139	50	0.0070	1.4841	0.0060	1.1252	0.0430	0.0067	0.5435	42.163
	104	142	50	0.0060	1.5156	0.0064	1.2822	0.0841	0.0094	0.6300	45.920
	116	138	50	0.0084	1.6033	0.0065	1.4074	0.1215	0.0074	0.7068	49.973
Y0G30H01T	84	132	125	0.0074	0.6819	0.0071	0.8389	0.0507	0.0122	0.4136	28.191
Y0G30H02T	62	125	125	0.0076	0.6589	0.0074	0.5007	0.0089	0.0125	0.2420	21.546
	51	115	125	0.0066	0.6170	0.0078	0.3467	0.0119	0.0122	0.1868	18.517
Y0G30H03T	110	121	125	0.0072	0.8089	0.0080	1.1530	0.2741	0.0145	0.5892	39.147
	96	129	125	0.0065	0.7156	0.0090	0.9756	0.1378	0.0127	0.4998	32.401
	82	131	125	0.0079	0.7052	0.0067	0.7600	0.0367	0.0105	0.4034	27.144
Y0G30L01T	17	145	159	0.0057	0.4185	0.0058	0.1622	[illegible]	0.0061	0.0813	10.869

Appen[illegible] - Table I: Sky Background Count Rates for G160L + Blue [illegible]con.

File Name	SEA	ETA	SA	100	0 order	800	Lyα	O I	Spectrum	Lyα	array
Y0G30L02T	12	170	159	0.0103	0.4381	0.0082	0.1467	0.0093	0.0107	0.0857	12.964
	30	162	159	0.0121	0.4385	0.0100	0.1819	0.0093	0.0127	0.1036	14.227
Y0G30L03T	45	116	159	0.0045	0.4337	0.0035	0.2478	0.0059	0.0058	0.1184	11.913
	26	136	159	0.0046	0.4348	0.0060	0.1637	0.0111	0.0078	0.0960	11.292
	10	155	159	0.0076	0.4248	0.0085	0.1556	0.0063	0.0086	0.0827	11.877
Y0G31H01T	64	139	77	0.0073	0.7793	0.0062	0.4811	0.0104	0.0076	0.2447	21.634
Y0G31H02T	91	165	77	0.0057	0.7944	0.0055	0.8133	0.0467	0.0109	0.3970	28.519
	108	162	77	0.0077	0.8337	0.0075	1.0159	0.0970	0.0077	0.4870	32.845
Y0G31H03T	42	111	77	0.0110	0.7837	0.0105	0.3122	0.0152	0.0127	0.1540	20.591
	56	130	77	0.0088	0.8174	0.0090	0.4419	0.0119	0.0109	0.1944	22.346
	72	148	77	0.0067	0.7944	0.0075	0.5833	0.0141	0.0085	0.2693	24.100
Y0G31J01T	30	115	91	0.0053	0.6174	0.0050	0.2574	0.0085	0.0073	0.1290	15.076
Y0G31J02T	62	128	91	0.0090	0.6641	0.0092	0.4963	0.0141	0.0123	0.2750	22.303
	81	129	91	0.0130	0.6948	0.0123	0.7759	0.0367	0.0148	0.3819	29.145
Y0G31J03T	12	98	91	0.0059	0.5915	0.0056	0.1904	0.0104	0.0080	0.1014	14.075
	22	110	91	0.0049	0.5978	0.0064	0.2344	0.0085	0.0081	0.1076	14.720
	40	120	91	0.0073	0.6159	0.0070	0.2885	0.0115	0.0069	0.1490	16.409
Y0G32101T	37	139	118	0.0077	0.3863	0.0061	0.2218	0.0104	0.0073	0.1163	12.107
Y0G32102T	59	166	118	0.0095	0.3896	0.0089	0.3722	0.0122	0.0081	0.1956	16.029
	75	164	118	0.0096	0.4419	0.0071	0.5296	0.0189	0.0093	0.2670	19.440
Y0G32103T	30	111	119	0.0046	0.3781	0.0046	0.1822	0.0107	0.0058	0.0881	10.492
	33	130	119	0.0062	0.3770	0.0061	0.2081	0.0074	0.0068	0.1002	11.436
	43	149	119	0.0073	0.4052	0.0082	0.2633	0.0122	0.0088	0.1354	13.768

- All count rates are in count/second/diode except for the counts under "array." These are in counts/second/array. No background subtraction has been done.
- The rates for the narrow features are based on an average of 36 pixels. (The first Lyα column and the O I rates are from the first order while the second Lyα column is from the second order.)
- The rates for the background are based on 401 pixels beginning at the pixel indicated in the column heading.
- The rate for the spectrum is based on 401 pixels (1500-1900) which excludes the geocoronal lines.
- The effect of noisy channels which were not disabled, if any, has been removed from the rates for the background and the spectrum count rates only.

Appendix Table II. Sky Background Count Rates For G160L + Red Digicon

File Name	SEA	ETA	SA	spectrum	800	0 order	1500	array
Y0G11901T	31	119	124	0.0099	0.0095	1.210	0.0105	20.124
	21	122	124	0.0098	0.0106	1.248	0.0083	20.119
Y0G11902T	3	125	124	0.0120	0.0090	1.169	0.0082	20.260
	5	125	124	0.0098	0.0065	1.215	0.0103	18.993
	11	124	124	0.0148	0.0142	1.164	0.0102	21.256
	19	122	124	0.0107	0.0089	1.194	0.0104	19.251
	27	119	124	0.0122	0.0121	1.173	0.0123	20.192
Y0G11903T	64	104	124	0.0166	0.0158	1.308	0.0160	24.239
	55	108	124	0.0145	0.0115	1.211	0.0117	21.314
	46	113	124	0.0175	0.0139	1.224	0.0157	22.784
	38	116	124	0.0138	0.0122	1.196	0.0120	20.949
	29	120	124	0.0127	0.0103	1.192	0.0108	20.036
	20	122	124	0.0149	0.0131	1.177	0.0099	21.772
	12	124	124	0.0105	0.0108	1.185	0.0090	19.336
Y0G11B01T	37	129	100	0.0180	0.0194	1.210	0.0193	24.052
	47	136	100	0.0167	0.0165	1.159	0.0207	23.043
Y0G11B02T	69	147	100	0.0177	0.0148	1.240	0.0161	22.870
	77	149	100	0.0180	0.0192	1.207	0.0155	22.828
	85	148	100	0.0121	0.0149	1.212	0.0135	21.554
	93	146	100	0.0128	0.0143	1.271	0.0099	21.957
	101	143	100	0.0125	0.0118	1.345	0.0153	22.348
Y0G11B03T	6	102	100	0.0123	0.0107	1.214	0.0118	20.928
	14	109	100	0.0153	0.0153	1.227	0.0162	22.411
	22	117	100	0.0182	0.0150	1.263	0.0130	22.585
	31	124	100	0.0147	0.0179	1.212	0.0195	23.193
	39	130	100	0.0155	0.0193	1.179	0.0199	22.592
	48	136	100	0.0195	0.0177	1.126	0.0166	22.968
	57	142	100	0.0161	0.0160	1.238	0.0181	23.314
Y0G11C01T	15	122	131	0.0108	0.0117	1.321	0.0102	21.599
	6	127	131	0.0114	0.0100	1.296	0.0105	21.121
Y0G11C02T	11	133	131	0.0102	0.0099	1.381	0.0084	21.846
	20	134	131	0.0095	0.0081	1.349	0.0103	20.487
	28	133	131	0.0086	0.0088	1.389	0.0091	21.093
	36	132	131	0.0107	0.0093	1.323	0.0100	21.773
	44	129	131	0.0076	0.0106	1.363	0.0126	21.737
Y0G11C03T	47	102	131	0.0177	0.0187	1.365	0.0160	25.471
	38	108	131	0.0145	0.0135	1.397	0.0143	23.981
	29	113	131	0.0135	0.0140	1.322	0.0142	23.110
	21	118	131	0.0154	0.0239	1.325	0.0199	25.728
	12	123	131	0.0129	0.0123	1.329	0.0118	22.202
	5	127	131	0.0128	0.0108	1.273	0.0129	22.049
	2	130	131	0.0093	0.0089	1.368	0.0082	21.368
Y0G11F01T	81	123	74	0.0104	0.0127	2.508	0.0087	35.679
	90	129	74	0.0089	0.0092	2.621	0.0098	37.109
Y0G11F02T	112	140	74	0.0080	0.0137	2.765	0.0126	39.332
	120	141	74	0.0111	0.0129	2.883	0.0110	41.556
	127	141	74	0.0095	0.0086	2.846	0.0114	39.684
	134	140	74	0.0084	0.0087	2.973	0.0107	40.047
	142	138	74	0.0112	0.0087	3.008	0.0109	41.794
Y0G11F03T	50	99	74	0.0074	0.0086	2.309	0.0088	32.199
	59	106	74	0.0083	0.0090	2.190	0.0097	32.190
	67	112	74	0.0094	0.0092	2.345	0.0094	33.476
	75	119	74	0.0100	0.0107	2.410	0.0098	34.998
	83	125	74	0.0083	0.0097	2.485	0.0127	35.508
	92	130	74	0.0095	0.0103	2.501	0.0134	35.923
	100	135	74	0.0117	0.0104	2.496	0.0126	35.432
Y0G11O01T	8	83	91	0.0117	0.0103	2.573	0.0081	37.053
	13	80	91	0.0134	0.0075	2.627	0.0091	38.331
Y0G11O02T	170	96	91	0.0123	0.0092	4.931	0.0093	64.838
	167	99	91	0.0128	0.0110	4.175	0.0090	57.474
	161	101	91	0.0103	0.0078	4.055	0.0080	55.152
	153	103	91	0.0127	0.0066	3.894	0.0083	53.[illegible]95

Appe - Table II: Sky Background Count Rates For G160L + Red icon

File Name	SEA	ETA	SA	spectrum	800	0 order	1500	array
	146	105	91	0.0127	0.0076	3.937	0.0115	53.373
Y0G11O03T	122	109	91	0.0156	0.0089	3.747	0.0090	48.975
	114	109	91	0.0130	0.0097	3.833	0.0085	48.836
	105	109	91	0.0136	0.0109	3.619	0.0087	46.606
	94	108	91	0.0147	0.0118	3.568	0.0142	46.765
	83	106	91	0.0161	0.0137	3.339	0.0128	44.362
	74	105	91	0.0157	0.0112	3.225	0.0189	42.861
	65	103	91	0.0172	0.0124	3.040	0.0160	41.540
Y0G11P01T	53	101	62	0.0118	0.0104	1.614	0.0111	25.055
	61	102	62	0.0109	0.0083	1.633	0.0088	24.567
Y0G11P02T	80	104	62	0.0098	0.0095	1.784	0.0140	27.329
	87	104	62	0.0094	0.0133	1.929	0.0098	29.300
	93	103	62	0.0120	0.0084	2.249	0.0119	32.251
	100	103	62	0.0130	0.0115	2.527	0.0101	36.315
	107	102	62	0.0093	0.0114	2.692	0.0086	37.166
Y0G11P03T	30	87	62	0.0115	0.0103	1.659	0.0141	27.085
	28	89	62	0.0082	0.0085	1.621	0.0149	28.057
	29	91	62	0.0127	0.0095	1.683	0.0110	26.082
	32	93	62	0.0119	0.0094	1.572	0.0075	24.457
	36	95	62	0.0082	0.0098	1.633	0.0093	25.552
	40	97	62	0.0090	0.0128	1.564	0.0097	26.843
	46	99	62	0.0080	0.0081	1.615	0.0101	24.757
Y0G11R01T	171	125	59	0.0108	0.0126	3.837	0.0126	53.309
	163	125	59	0.0083	0.0073	3.721	0.0097	51.367
Y0G11R02T	142	120	59	0.0111	0.0112	4.153	0.0084	57.774
	134	117	59	0.0131	0.0116	3.816	0.0110	55.366
	126	113	59	0.0121	0.0117	4.037	0.0088	57.112
	118	110	59	0.0091	0.0092	3.971	0.0144	56.911
	110	105	59	0.0135	0.0151	4.132	0.0121	60.352
Y0G11R03T	122	104	59	0.0087	0.0096	4.575	0.0064	58.802
	130	108	59	0.0101	0.0071	4.459	0.0070	56.264
	139	112	59	0.0080	0.0107	4.156	0.0061	53.325
	148	116	59	0.0091	0.0086	4.234	0.0114	53.916
	156	120	59	0.0081	0.0093	4.122	0.0089	52.963
	165	122	59	0.0082	0.0102	3.993	0.0098	51.760
	172	124	59	0.0125	0.0119	3.773	0.0091	50.880
Y0G11W01T	155	144	56	0.0218	0.0142	4.912	0.0195	68.593
	145	153	56	0.0174	0.0185	4.862	0.0168	67.567
Y0G11W02T	123	164	56	0.0102	0.0121	4.761	0.0093	63.100
	115	162	56	0.0111	0.0088	4.809	0.0114	63.751
	107	157	56	0.0187	0.0133	4.666	0.0124	65.363
	96	148	56	0.0174	0.0151	4.625	0.0162	66.293
	85	138	56	0.0166	0.0140	4.755	0.0197	65.759
Y0G11W03T	169	114	55	0.0167	0.0218	5.645	0.0213	78.773
	173	123	55	0.0145	0.0148	5.419	0.0162	72.991
	169	131	55	0.0193	0.0173	5.217	0.0197	71.902
	161	139	55	0.0176	0.0188	5.082	0.0224	72.170
	152	147	55	0.0153	0.0140	5.075	0.0177	69.304
	144	154	55	0.0203	0.0144	4.921	0.0213	69.508
	135	160	55	0.0148	0.0185	4.840	0.0181	68.108
Y0G12101T	80	96	149	0.0096	0.0094	2.129	0.0099	31.220
	71	106	149	0.0124	0.0125	2.053	0.0119	30.849
Y0G12102T	50	128	149	0.0099	0.0105	1.750	0.0108	26.480
	43	136	149	0.0131	0.0110	1.704	0.0115	26.428
	36	143	149	0.0088	0.0125	1.671	0.0110	26.159
	30	151	149	0.0121	0.0111	1.659	0.0163	26.853
	25	158	149	0.0114	0.0155	1.681	0.0131	27.161
Y0G12103T	32	149	149	0.0118	0.0129	1.485	0.0125	24.578
	32	148	149	0.0119	0.0119	1.530	0.0118	25.154
	32	149	149	0.0091	0.0105	1.599	0.0096	23.996
	33	148	149	0.0113	0.0088	1.663	0.0110	24.663
	34	148	149	0.0103	0.0082	1.559	0.0083	23.037

File Name	SEA	ETA	SA	spectrum	800	0 order	1500	array
	37	146	149	0.0118	0.0103	1.532	0.0112	24.079
	40	142	149	0.0086	0.0082	1.554	0.0079	23.637
Y0G12201T	31	128	102	0.0114	0.0118	1.424	0.0131	23.574
	26	127	102	0.0101	0.0100	1.485	0.0128	24.305
Y0G12202T	25	120	102	0.0135	0.0116	1.360	0.0126	22.944
	28	117	102	0.0113	0.0130	1.435	0.0111	23.993
	32	113	102	0.0124	0.0121	1.442	0.0143	24.313
	38	109	102	0.0119	0.0133	1.514	0.0258	27.015
	43	104	102	0.0160	0.0182	1.502	0.0228	27.283
Y0G12203T	89	104	102	0.0259	0.0190	1.664	0.0223	31.557
	82	110	102	0.0218	0.0179	1.512	0.0186	28.504
	74	115	102	0.0195	0.0162	1.534	0.0114	26.766
	66	119	102	0.0150	0.0152	1.512	0.0172	26.450
	56	123	102	0.0151	0.0124	1.480	0.0118	24.636
	45	126	102	0.0151	0.0165	1.522	0.0178	26.719
	38	128	102	0.0115	0.0080	1.469	0.0119	23.344
Y0G12401T	48	95	149	0.0102	0.0096	2.001	0.0103	30.197
	39	105	149	0.0094	0.0098	1.990	0.0126	29.801
Y0G12402T	22	127	149	0.0118	0.0098	2.010	0.0090	29.632
	18	135	149	0.0115	0.0094	1.987	0.0101	30.190
	18	142	149	0.0095	0.0119	1.968	0.0101	29.220
	19	150	149	0.0117	0.0108	2.010	0.0118	30.023
	22	156	149	0.0096	0.0092	2.008	0.0094	29.337
Y0G12403T	34	146	149	0.0092	0.0124	1.840	0.0099	27.516
	37	147	149	0.0098	0.0085	1.800	0.0101	27.047
	41	147	149	0.0097	0.0095	1.846	0.0099	27.120
	46	147	149	0.0132	0.0105	1.831	0.0096	27.842
	55	147	149	0.0128	0.0099	1.798	0.0088	26.515
	62	144	149	0.0088	0.0105	1.944	0.0087	27.983
	70	138	149	0.0099	0.0108	2.046	0.0116	29.754
Y0G12501T	160	147	50	0.0104	0.0106	2.895	0.0103	40.695
	151	157	50	0.0100	0.0108	2.756	0.0098	38.345
Y0G12502T	124	173	50	0.0136	0.0143	2.791	0.0112	41.279
	116	166	50	0.0117	0.0130	2.675	0.0110	38.793
	108	158	50	0.0093	0.0107	2.718	0.0116	39.052
	100	150	50	0.0108	0.0112	2.663	0.0123	38.240
	92	142	50	0.0121	0.0100	2.669	0.0127	39.028
Y0G12503T	161	115	50	0.0106	0.0078	3.654	0.0093	49.049
	167	124	50	0.0097	0.0106	3.281	0.0086	44.658
	169	132	50	0.0112	0.0101	3.169	0.0094	42.975
	165	141	50	0.0106	0.0110	2.916	0.0113	40.192
	158	150	50	0.0099	0.0087	2.844	0.0102	39.547
	150	158	50	0.0132	0.0127	2.656	0.0098	38.831
	139	169	50	0.0115	0.0116	2.691	0.0098	38.754
Y0G12602R	90	94	107	0.0104	0.0086	2.532	0.0091	35.592
	98	95	107	0.0092	0.0096	2.543	0.0087	35.838
	105	96	107	0.0091	0.0069	2.547	0.0079	35.129
	112	97	107	0.0103	0.0070	2.866	0.0101	39.170
	119	98	107	0.0100	0.0086	3.073	0.0075	41.735
Y0G12603R	138	100	107	0.0096	0.0074	3.475	0.0085	46.199
	143	100	107	0.0124	0.0144	3.574	0.0099	49.350
	148	100	107	0.0133	0.0098	3.605	0.0114	49.861
	151	99	107	0.0150	0.0101	3.724	0.0088	50.574
	151	99	107	0.0142	0.0105	3.976	0.0120	54.937
	150	98	107	0.0172	0.0130	4.645	0.0123	63.097
	146	96	107	0.0158	0.0102	4.562	0.0111	62.458
Y0G12901T	40	76	106	0.0178	0.0131	1.609	0.0130	26.852
	34	76	106	0.0194	0.0138	1.573	0.0172	27.704
Y0G12902T	28	79	106	0.0256	0.0183	1.490	0.0181	28.325
	29	80	106	0.0247	0.0196	1.463	0.0209	28.153
	32	81	106	0.0249	0.0156	1.337	0.0152	25.745
	37	83	106	0.0196	0.0139	1.319	0.0175	[illegible]

Appe - Table II: Sky Background Count Rates For G160L + Red icon

File Name	SEA	ETA	SA	spectrum	800	0 order	1500	array
	42	84	106	0.0193	0.0122	1.230	0.0144	23.198
Y0G12903T	61	89	106	0.0126	0.0130	1.168	0.0199	21.774
	69	91	106	0.0110	0.0102	1.238	0.0108	20.320
	76	92	106	0.0093	0.0080	1.423	0.0085	22.417
	84	94	106	0.0105	0.0094	1.795	0.0090	26.898
	92	96	106	0.0072	0.0098	1.856	0.0112	28.039
	100	97	106	0.0083	0.0088	2.136	0.0083	30.074
	107	99	106	0.0102	0.0089	2.167	0.0070	30.522
Y0G12D01T	84	137	132	0.0135	0.0137	2.228	0.0164	49.740
	75	142	132	0.0100	0.0193	2.073	0.0139	35.956
Y0G12D02T	57	144	132	0.0083	0.0081	1.976	0.0080	28.778
	51	142	132	0.0117	0.0113	1.981	0.0087	30.418
	46	139	132	0.0082	0.0095	1.959	0.0077	28.737
	41	135	132	0.0105	0.0100	1.914	0.0088	29.668
	36	130	132	0.0106	0.0095	1.932	0.0082	299.983
Y0G12D03T	117	109	132	0.0134	0.0149	3.045	0.0148	43.752
	109	116	132	0.0182	0.0156	2.654	0.0136	40.045
	102	123	132	0.0152	0.0125	2.251	0.0128	33.898
	92	131	132	0.0141	0.0120	2.140	0.0152	32.750
	82	138	132	0.0132	0.0151	2.148	0.0122	32.713
	74	142	132	0.0113	0.0139	2.062	0.0122	31.451
	67	144	132	0.0100	0.0095	2.014	0.0121	29.798
Y0G12E01T	84	145	129	0.0107	0.0113	2.161	0.0107	31.553
	76	151	129	0.0101	0.0094	2.030	0.0087	29.717
Y0G12E02T	58	155	129	0.0093	0.0073	1.798	0.0096	26.253
	52	152	129	0.0088	0.0132	1.769	0.0082	26.289
	46	147	129	0.0088	0.0078	1.757	0.0107	26.276
	41	142	129	0.0069	0.0063	1.748	0.0071	25.313
	37	135	129	0.0075	0.0074	1.830	0.0063	25.911
Y0G12E03T	116	112	129	0.0075	0.0070	2.282	0.0082	32.070
	109	120	129	0.0087	0.0071	2.131	0.0070	29.800
	102	128	129	0.0089	0.0076	2.014	0.0106	28.794
	92	138	129	0.0096	0.0092	1.940	0.0080	28.280
	82	147	129	0.0095	0.0087	1.878	0.0074	27.127
	75	152	129	0.0083	0.0081	1.943	0.0090	28.124
	68	155	129	0.0078	0.0088	1.787	0.0064	25.893
Y0G12M01T	32	138	140	0.0080	0.0130	1.719	0.0104	26.283
	35	145	140	0.0115	0.0097	1.801	0.0118	27.109
Y0G12M02T	46	156	140	0.0128	0.0118	1.783	0.0140	28.373
	51	156	140	0.0110	0.0142	1.737	0.0130	27.653
	57	154	140	0.0115	0.0125	1.701	0.0102	26.030
	63	149	140	0.0107	0.0103	1.762	0.0091	26.690
	69	144	140	0.0129	0.0094	1.781	0.0110	26.919
Y0G12M03T	40	109	140	0.0102	0.0084	1.648	0.0101	25.408
	35	117	140	0.0090	0.0100	1.810	0.0100	27.183
	32	125	140	0.0083	0.0068	1.724	0.0090	26.466
	32	133	140	0.0104	0.0104	1.804	0.0120	27.288
	33	140	140	0.0117	0.0090	1.690	0.0107	26.045
	36	146	140	0.0179	0.0170	1.697	0.0194	30.187
	39	152	140	0.0103	0.0107	1.840	0.0100	27.429
Y0G20201T	65	130	67	0.0146	0.0120	2.169	0.0147	35.855
	74	138	67	0.0148	0.0174	2.134	0.0160	36.452
Y0G20202T	94	149	67	0.0173	0.0162	2.229	0.0186	38.329
	102	151	67	0.0188	0.0176	2.285	0.0212	39.190
	109	150	67	0.0175	0.0156	2.148	0.0167	36.525
	116	148	67	0.0156	0.0186	2.237	0.0147	37.510
	124	144	67	0.0156	0.0121	2.369	0.0135	37.340
Y0G20203T	37	103	67	0.0117	0.0112	2.151	0.0103	34.431
	44	111	67	0.0103	0.0116	2.131	0.0095	33.857
	51	118	67	0.0140	0.0096	2.142	0.0093	34.349
	59	125	67	0.0123	0.0086	2.053	0.0099	32.949
	67	132	67	0.0138	0.0100	2.153	0.0118	34.425

File Name	SEA	ETA	SA	spectrum	800	0 order	1500	array
	75	139	67	0.0116	0.0134	2.115	0.0147	35.149
	83	144	67	0.0168	0.0157	2.231	0.0145	37.243
Y0G20401T	78	132	54	0.0146	0.0119	3.111	0.0101	44.255
	88	140	54	0.0117	0.0101	3.050	0.0100	42.671
Y0G20402T	108	153	54	0.0134	0.0097	3.109	0.0128	44.012
	115	154	54	0.0127	0.0127	3.162	0.0108	44.478
	122	154	54	0.0136	0.0104	3.147	0.0095	44.137
	129	151	54	0.0127	0.0113	3.153	0.0110	43.972
	136	146	54	0.0117	0.0089	3.156	0.0113	44.023
Y0G20403T	50	104	54	0.0110	0.0093	3.093	0.0106	42.810
	57	112	54	0.0126	0.0085	2.964	0.0087	42.123
	65	120	54	0.0137	0.0110	3.095	0.0126	43.713
	73	127	54	0.0125	0.0120	3.092	0.0153	44.089
	81	134	54	0.0100	0.0092	3.062	0.0108	42.870
	89	141	54	0.0144	0.0098	3.075	0.0119	43.742
	97	147	54	0.0122	0.0109	3.176	0.0109	44.361
Y0G20801T	55	129	80	0.0099	0.0087	1.850	0.0083	27.026
	65	136	80	0.0082	0.0077	1.863	0.0101	27.540
Y0G20802T	87	147	80	0.0119	0.0111	1.816	0.0113	28.307
	95	148	80	0.0128	0.0104	1.905	0.0112	28.862
	103	147	80	0.0124	0.0111	1.940	0.0117	29.980
	111	145	80	0.0121	0.0088	1.941	0.0099	28.511
	119	141	80	0.0106	0.0099	1.967	0.0153	30.248
Y0G20803T	23	103	80	0.0107	0.0086	1.916	0.0094	29.398
	32	110	80	0.0122	0.0108	1.908	0.0102	28.594
	40	117	80	0.0088	0.0093	1.813	0.0092	27.284
	49	124	80	0.0109	0.0091	1.815	0.0103	27.498
	57	131	80	0.0109	0.0095	1.805	0.0086	27.204
	66	137	80	0.0118	0.0072	1.816	0.0134	27.520
	75	142	80	0.0098	0.0078	2.041	0.0101	29.573
Y0G20W01T	42	86	114	0.0174	0.0110	3.090	0.0100	44.091
	33	89	114	0.0172	0.0084	2.851	0.0097	43.512
Y0G20W02T	17	98	114	0.0183	0.0117	2.819	0.0103	41.280
	14	100	114	0.0137	0.0103	2.859	0.0108	41.444
	13	103	114	0.0181	0.0100	2.814	0.0107	41.892
	19	105	114	0.0171	0.0089	2.885	0.0116	41.752
	28	106	114	0.0170	0.0135	2.794	0.0151	41.469
Y0G20W03T	34	104	114	0.0160	0.0109	2.657	0.0107	38.745
	37	106	114	0.0156	0.0105	2.591	0.0101	39.292
	45	106	114	0.0180	0.0087	2.605	0.0104	37.991
	52	106	114	0.0171	0.0128	2.611	0.0106	38.214
	59	107	114	0.0180	0.0111	2.593	0.0101	38.626
	67	106	114	0.0165	0.0083	2.810	0.0094	40.791
	74	106	114	0.0145	0.0136	3.163	0.0109	43.640
Y0G20Y01T	39	87	115	0.0213	0.0128	3.046	0.0189	45.664
	30	91	115	0.0193	0.0098	3.014	0.0138	42.731
Y0G20Y02T	15	99	115	0.0166	0.0108	2.916	0.0130	42.360
	12	102	115	0.0172	0.0124	2.981	0.0103	43.292
	16	104	115	0.0167	0.0103	3.009	0.0095	43.052
	23	106	115	0.0167	0.0102	3.177	0.0113	44.315
	30	107	115	0.0161	0.0088	3.177	0.0101	43.673
Y0G20Y03T	34	106	115	0.0161	0.0093	2.954	0.0095	41.264
	38	107	115	0.0173	0.0106	3.059	0.0113	43.717
	46	107	115	0.0226	0.0180	3.060	0.0144	47.656
	54	108	115	0.0212	0.0120	4.414	0.0104	63.317
	61	107	115	0.0194	0.0142	9.341	0.0135	113.517
	69	107	115	0.0240	0.0166	24.989	0.0150	257.546
	76	106	115	0.0243	0.0160	26.212	0.0182	266.599
Y0G22001T	58	150	119	0.0203	0.0169	5.553	0.0186	67.733
	53	158	119	0.0196	0.0149	5.265	0.0176	63.691
Y0G22002T	46	165	119	0.0168	0.0175	5.544	0.0160	66.182
	45	161	119	0.0159	0.0135	5.345	0.0137	[illegible]

- All count rates are in count/second/diode except for the counts under "array." These are in counts/second/array. No background subtraction has been done.
- The rates for the narrow features are based on an average of 36 pixels.
- The rates for the background are based on 401 pixels beginning at the pixel indicated in the column heading.
- The rate for the spectrum is based on 401 pixels (100-500).
- The effect of noisy channels which were not disabled, if any, has been removed from the rates for the background and the spectrum count rates only.

File Name	RA	DEC	ℓ^{II}	b^{II}	λ	β	$\lambda_{\odot}$	SEA	ETA	SA	Peak	spectrum	900	0 order	1600	array
YOG11904T	11.08	-58.46	304	-58	25	-55	151	14	122	124	0.1117	0.0660	0.0096	0.0744	0.0099	17.894
YOG11905T	11.08	-58.46	304	-58	25	-55	151	58	111	124	0.1190	0.0715	0.0130	0.0704	0.0137	20.208
YOG11906T	11.08	-58.46	304	-58	25	-55	151	38	106	124	0.1215	0.0751	0.0149	0.0757	0.0164	21.644
YOG11B04T	13.51	-51.14	301	-65	16	-50	90	89	147	100	0.1138	0.0724	0.0126	0.0767	0.0139	20.412
YOG11B05T	13.51	-51.14	301	-65	16	-50	90	132	130	100	0.1620	0.0935	0.0092	0.0843	0.0093	23.858
YOG11B06T	13.51	-51.14	301	-65	16	-50	90	62	131	100	0.1238	0.0723	0.0161	0.0731	0.0172	21.393
YOG11C04T	17.95	-40.49	287	-76	3	-43	152	31	132	131	0.1257	0.0724	0.0111	0.0637	0.0094	19.487
YOG11C05T	17.95	-40.49	287	-76	3	-43	152	75	120	131	0.1313	0.0768	0.0112	0.0743	0.0112	20.715
YOG11C06T	17.95	-40.49	287	-76	3	-43	152	13	116	131	0.1310	0.0746	0.0114	0.0741	0.0111	20.170
YOG11F04T	40.89	-10.87	186	-59	34	-25	107	130	141	74	0.2410	0.1448	0.0075	0.1359	0.0097	35.590
YOG11F05T	40.89	-10.87	186	-59	34	-25	107	158	128	74	0.2740	0.1587	0.0096	0.1496	0.0097	38.813
YOG11F06T	40.89	-10.87	186	-59	34	-25	107	75	102	74	0.2194	0.1233	0.0104	0.1212	0.0108	31.030
YOG11O04T	85.68	-68.10	278	-31	44	-87	104	34	95	91	0.2403	0.1311	0.0099	0.1322	0.0104	33.114
YOG11O05T	85.68	-68.10	278	-31	44	-87	104	159	98	91	0.4106	0.2332	0.0094	0.2291	0.0086	56.018
YOG11O06T	85.68	-68.10	278	-31	44	-87	104	94	109	91	0.2593	0.1548	0.0126	0.1872	0.0116	38.944
YOG11P04T	123.71	75.97	138	31	103	54	65	71	104	62	0.1597	0.0915	0.0100	0.0952	0.0115	23.984
YOG11P05T	123.71	75.97	138	31	103	54	65	108	103	62	0.2342	0.1294	0.0096	0.1209	0.0113	32.488
YOG11P06T	123.71	75.97	138	31	103	54	65	35	88	62	0.1549	0.0885	0.0108	0.0852	0.0097	23.148
YOG11R04T	140.30	80.28	132	32	104	59	97	152	123	59	0.3093	0.1767	0.0091	0.1541	0.0093	42.647
YOG11R05T	140.30	80.28	132	32	104	59	97	107	111	59	0.3403	0.1933	0.0108	0.1772	0.0091	46.707
YOG11R06T	140.30	80.28	132	32	104	59	97	147	106	59	0.3190	0.1794	0.0094	0.1786	0.0094	43.489
YOG11W04T	150.09	0.54	238	41	151	-10	96	171	120	55	0.4864	0.2666	0.0128	0.2578	0.0137	64.283
YOG11W05T	150.09	0.54	238	41	151	-10	96	138	149	55	0.4503	0.2495	0.0148	0.2433	0.0129	60.862
YOG11W06T	150.09	0.54	238	41	151	-10	96	158	118	55	0.4526	0.2506	0.0114	0.2525	0.0111	60.354
YOG12104T	163.10	38.57	180	62	148	28	339	79	98	149	0.1710	0.1029	0.0130	0.1119	0.0125	27.251
YOG12105T	163.10	38.57	180	62	148	28	339	40	128	149	0.1612	0.0915	0.0118	0.0915	0.0124	24.367
YOG12106T	163.10	38.57	180	62	148	28	339	34	149	149	0.1496	0.0827	0.0112	0.0810	0.0110	23.821
YOG12204T	184.49	33.94	168	79	191	32	63	24	124	102	0.1465	0.0829	0.0118	0.0822	0.0111	22.386
YOG12205T	184.49	33.94	168	79	191	32	63	45	110	102	0.1455	0.0853	0.0145	0.0841	0.0139	23.477
YOG12206T	184.49	33.94	168	79	191	32	63	64	107	102	0.1461	0.0876	0.0171	0.0933	0.0167	25.011
YOG12404T	188.57	13.33	285	75	182	15	335	47	97	149	0.1844	0.1034	0.0107	0.1067	0.0085	26.282
YOG12405T	188.57	13.33	285	75	182	15	335	20	128	149	0.1852	0.1034	0.0108	0.1041	0.0098	26.525
YOG12406T	188.57	13.33	285	75	182	15	335	47	146	149	0.1734	0.0967	0.0098	0.0985	0.0097	24.774
YOG12504T	194.57	30.21	98	86	180	33	139	104	154	50	0.2692	0.1447	0.0120	0.1437	0.0102	36.193
YOG12505T	194.57	30.21	98	86	180	33	139	61	123	50	0.2579	0.1422	0.0103	0.1367	0.0106	35.372
YOG12506T	194.57	30.21	98	86	180	33	139	158	119	50	0.2748	0.1533	0.0114	0.1494	0.0096	37.876
YOG12604R	198.54	70.56	120	46	221	65	2	123	90	107	0.3907	0.2412	0.0137	0.2363	0.0135	58.820
YOG12605T	198.54	70.56	120	46	221	65	2	73	89	107	0.1274	0.0994	0.0117	0.0822	0.0104	25.678
YOG12606T	198.54	70.56	120	46	221	65	2	129	98	107	0.2623	0.1570	0.0092	0.1311	0.0087	38.007
YOG12904T	205.71	71.29	117	45	220	67	1	134	101	106	0.2511	0.1408	0.0126	0.1263	0.0132	37.103
YOG12905T	205.71	71.29	117	45	220	67	1	149	101	106	0.3186	0.1938	0.0174	0.1783	0.0181	49.175
YOG12906T	205.71	71.29	117	45	220	67	1	40	80	106	0.1216	0.0743	0.0154	0.0760	0.0157	21.414
YOG12D04T	215.20	-7.88	337	48	215	5	82	43	137	132	0.1933	0.1055	0.0097	0.1004	0.0097	26.779
YOG12D05T	215.20	-7.88	337	48	215	5	82	31	116	132	0.1883	0.1040	0.0081	0.1006	0.0079	26.000
YOG12D06T	215.20	-7.88	337	48	215	5	82	92	113	132	0.2053	0.1262	0.0137	0.1222	0.0139	32.684
YOG12E04T	217.15	3.57	351	57	213	17	82	44	145	129	0.1589	0.0938	0.0085	0.0952	0.0094	24.053
YOG12E05T	217.15	3.57	351	57	213	17	82	32	119	129	0.1676	0.0946	0.0101	0.0937	0.0078	24.090
YOG12E06T	217.15	3.57	351	57	213	17	82	92	116	129	0.1706	0.1020	0.0086	0.0977	0.0093	25.768
YOG12M04T	326.17	1.75	57	-36	328	14	112	60	152	140	0.1603	0.0943	0.0197	0.1070	0.0109	26.427
YOG12M05T	326.17	1.75	57	-36	328	14	112	95	128	140	0.1852	0.1016	0.0121	0.0976	0.0115	26.573
YOG12M06T	326.17	1.75	57	-36	328	14	112	35	113	140	0.1667	0.0931	0.0113	0.0946	0.0121	24.488
YOG20204T	28.81	56.41	131	-5	49	41	108	112	149	67	0.2289	0.1319	0.0160	0.1130	0.0164	34.477
YOG20205T	28.81	56.41	131	-5	49	41	108	50	106	67	0.2063	0.1202	0.0094	0.1072	0.0095	29.943
YOG20206T	28.81	56.41	131	-5	49	41	108	110	148	67	0.2174	0.1278	0.0138	0.1199	0.0121	32.963
YOG20404T	50.01	49.03	146	-6	61	29	109	126	152	54	0.2893	0.1582	0.0104	0.1430	0.0092	38.600
YOG20405T	50.01	49.03	146	-6	61	29	109	153	132	54	0.3270	0.1820	0.0106	0.1731	0.0093	44.252
YOG20406T	50.01	49.03	146	-6	61	29	109	73	108	54	0.2761	0.1561	0.0093	0.1621	0.0102	38.450
YOG20804T	67.73	59.89	147	7	76	37	154	107	146	80	0.1736	0.1018	0.0099	0.1052	0.0125	26.352
YOG20805T	67.73	59.89	147	7	76	37	154	149	129	80	0.2251	0.1268	0.0095	0.1257	0.0113	31.753
YOG20806T	67.73	59.89	147	7	76	37	154	49	106	80	0.1656	0.0963	0.0093	0.1078	0.0092	24.650
YOG20W04T	162.14	-58.74	287	0	158	-57	343	132	93	114	0.4836	0.2772	0.0120	0.2304	0.0122	65.943
YOG20W[illegible]	162.14	-58.74	287	0	158	-57	343	33	85	114	0.2335	0.1378	0.0100	0.1465	0.0104	34.417

File Name	RA	DEC	ℓ^{II}	b^{II}	λ	β	$\lambda_{\odot}$	SEA	ETA	SA	100	600	1100	Peak	spectrum	array
Y0G20Y08T	162.27	-58.68	287	0	158	-57	343	135	96	115	0.0197	0.0210	0.0238	4.6559	1.8255	149.152
Y0G20Y09T	162.27	-58.68	287	0	158	-57	343	48	78	115	0.0165	0.0163	0.0161	1.8233	0.6851	59.458
Y0G22007T	300.27	40.83	76	5	318	59	122	44	151	119	0.0133	0.0152	0.0156	2.3851	0.7909	66.690
Y0G22008T	300.27	40.83	76	5	318	59	122	60	122	119	0.0125	0.0133	0.0148	2.8928	0.9523	78.355
Y0G22009T	300.27	40.83	76	5	318	59	122	63	123	119	0.0128	0.0131	0.0149	2.5532	0.8469	70.351
Y0G22207T	300.59	36.20	72	2	315	54	123	67	98	124	0.0112	0.0103	0.0105	1.4177	0.5042	43.147
Y0G22208T	300.59	36.20	72	2	315	54	123	69	124	124	0.0084	0.0090	0.0106	1.3747	0.5141	43.503
Y0G22209T	300.59	36.20	72	2	315	54	123	46	169	124	0.0117	0.0121	0.0137	1.3868	0.5071	44.136
Y0G22407T	300.92	23.72	62	-3	309	43	123	43	154	136	0.0098	0.0090	0.0103	1.3377	0.4248	36.587
Y0G22408T	300.92	23.72	62	-3	309	43	123	60	123	136	0.0103	0.0098	0.0109	1.3155	0.4361	37.613
Y0G22409T	300.92	23.72	62	-3	309	43	123	62	125	136	0.0113	0.0134	0.0124	1.3180	0.4397	38.880
Y0G30207T	58.07	26.05	166	-21	61	5	123	127	109	62	0.0137	0.0151	0.0170	3.9277	1.3260	107.317
Y0G30208T	58.07	26.05	166	-21	61	5	123	47	99	62	0.0099	0.0096	0.0118	3.3228	1.0542	84.528
Y0G30209T	58.07	26.05	166	-21	61	5	123	89	129	62	0.0128	0.0125	0.0144	3.3498	1.0936	88.593
Y0G30407T	63.37	18.13	175	-23	64	-3	187	77	137	122	0.0134	0.0139	0.0127	1.8444	0.6005	51.320
Y0G30408T	63.37	18.13	175	-23	64	-3	187	115	126	122	0.0105	0.0099	0.0102	2.1322	0.7062	58.127
Y0G30409T	63.37	18.13	175	-23	64	-3	187	35	101	122	0.0174	0.0167	0.0165	1.7744	0.5860	52.006
Y0G30607T	67.07	19.00	177	-20	68	-2	192	103	132	123	0.0082	0.0084	0.0081	2.0284	0.6460	52.703
Y0G30608T	67.07	19.00	177	-20	68	-2	192	59	143	123	0.0111	0.0108	0.0107	1.8714	0.6075	50.795
Y0G30609T	67.07	19.00	177	-20	68	-2	192	77	149	124	0.0094	0.0102	0.0092	1.9208	0.6205	51.242
Y0G30I07T	247.80	-23.32	354	16	249	-1	123	65	128	125	0.0128	0.0116	0.0126	2.0656	0.7308	61.430
Y0G30I08T	247.80	-23.32	354	16	249	-1	123	45	112	125	0.0146	0.0153	0.0171	2.1081	0.7418	63.468
Y0G30I09T	247.80	-23.32	354	16	249	-1	123	107	108	125	0.0103	0.0086	0.0103	2.3170	0.8228	67.257
Y0G32207T	40.66	17.62	156	-37	43	1	187	99	110	144	0.0126	0.0123	0.0111	1.7217	0.6042	51.027
Y0G32208T	40.66	17.62	156	-37	43	1	187	33	99	144	0.0116	0.0126	0.0113	1.4995	0.4846	41.863
Y0G32209T	40.66	17.62	156	-37	43	1	187	51	131	144	0.0161	0.0128	0.0128	1.4922	0.4874	42.991
Y0G32807T	195.05	-4.79	306	58	195	1	124	113	169	71	0.0099	0.0105	0.0113	2.9805	0.9428	75.997
Y0G32808T	195.05	-4.79	306	58	195	1	124	82	146	71	0.0110	0.0113	0.0110	2.9345	0.9481	76.563
Y0G32809T	195.05	-4.79	306	58	195	1	124	91	165	71	0.0110	0.0108	0.0112	2.9330	0.9457	76.334

- All count rates are in count/second/diode except for the counts under "array." These are in counts/second/array. No background subtraction has been done.
- The rates for the background are based on 401 pixels beginning at the pixel indicated in the column heading.
- The rates for the peak of the spectrum are based on 24 pixels (1918-1941).
- The rate for the spectrum is based on 301 pixels (1700-2000).
- The effect of noisy channels which were not disabled, if any, has been removed from the rates for the background count rates only.

File Name	RA	DEC	l^{II}	b^{II}	λ	β	$\lambda_{\odot}$	SEA	ETA	SA	Peak	spectrum	900	0 order	1600	array
YOG20W06T	162.14	-58.74	287	0	158	-57	343	32	96	114	0.2551	0.1832	0.0094	0.2480	0.0092	45.033
YOG20Y04T	162.27	-58.68	287	0	158	-57	343	133	93	115	0.5414	0.3240	0.0187	0.2974	0.0202	79.057
YOG20Y05T	162.27	-58.68	287	0	158	-57	343	33	85	115	0.2506	0.1459	0.0149	0.1469	0.0147	37.403
YOG20Y06T	162.27	-58.68	287	0	158	-57	343	31	97	115	0.2287	0.1338	0.0106	0.1425	0.0116	33.648
YOG22004T	300.27	40.83	76	5	318	59	122	44	151	119	0.3521	0.1919	0.0120	0.2881	0.0115	47.850
YOG22005T	300.27	40.83	76	5	318	59	122	60	122	119	0.3958	0.2107	0.0114	0.3322	0.0108	52.140
YOG22006T	300.27	40.83	76	5	318	59	122	63	123	119	0.3665	0.1976	0.0157	0.3036	0.0155	50.338
YOG22204T	300.59	36.20	72	2	315	54	123	44	153	124	0.2014	0.1185	0.0120	0.1315	0.0122	30.596
YOG22205T	300.59	36.20	72	2	315	54	123	69	123	124	0.1949	0.1158	0.0093	0.1285	0.0097	29.285
YOG22206T	300.59	36.20	72	2	315	54	123	46	169	124	0.1934	0.1179	0.0121	0.1186	0.0127	30.437
YOG22404T	300.92	23.72	62	-3	309	43	123	43	154	136	0.1690	0.1061	0.0095	0.1081	0.0095	26.902
YOG22405T	300.92	23.72	62	-3	309	43	123	60	122	136	0.1835	0.1038	0.0106	0.1109	0.0101	26.602
YOG22406T	300.92	23.72	62	-3	309	43	123	62	125	136	0.1789	0.1059	0.0119	0.1111	0.0126	27.694
YOG30204T	58.07	26.05	166	-21	61	5	123	127	109	62	0.5475	0.3000	0.0142	0.2781	0.0138	72.183
YOG30205T	58.07	26.05	166	-21	61	5	123	48	99	62	0.4437	0.2410	0.0107	0.2433	0.0099	57.770
YOG30206T	58.07	26.05	166	-21	61	5	123	89	129	62	0.4546	0.2527	0.0143	0.2494	0.0140	61.550
YOG30404T	63.37	18.13	175	-23	64	-3	186	77	137	122	0.2417	0.1403	0.0122	0.1300	0.0133	35.490
YOG30405T	63.37	18.13	175	-23	64	-3	186	115	126	122	0.2872	0.1605	0.0118	0.1589	0.0114	39.713
YOG30406T	63.37	18.13	175	-23	64	-3	187	35	101	122	0.2494	0.1441	0.0178	0.1465	0.0196	38.231
YOG30604T	67.07	19.00	177	-20	68	-2	192	86	145	123	0.2440	0.1417	0.0095	0.1478	0.0082	34.897
YOG30605T	67.07	19.00	177	-20	68	-2	192	121	123	123	0.3290	0.1849	0.0106	0.1787	0.0108	45.118
YOG30606T	67.07	19.00	177	-20	68	-2	192	56	132	123	0.2467	0.1429	0.0116	0.1484	0.0119	36.000
YOG30I04T	247.80	-23.32	354	16	249	-1	123	65	128	125	0.2832	0.1625	0.0130	0.1637	0.0143	40.930
YOG30I05T	247.80	-23.32	354	16	249	-1	123	45	112	125	0.2901	0.1667	0.0170	0.1687	0.0183	43.158
YOG30I06T	247.80	-23.32	354	16	249	-1	123	107	108	125	0.3091	0.1775	0.0086	0.1728	0.0095	43.037
YOG32204T	40.66	17.62	156	-37	43	1	187	52	134	144	0.2075	0.1165	0.0115	0.1152	0.0107	29.816
YOG32205T	40.66	17.62	156	-37	43	1	187	33	99	144	0.2055	0.1180	0.0120	0.1141	0.0117	30.100
YOG32206T	40.66	17.62	156	-37	43	1	187	51	131	144	0.2054	0.1155	0.0121	0.1207	0.0131	29.942
YOG32804T	195.05	-4.79	306	58	195	1	124	82	135	71	0.4053	0.2189	0.0113	0.2248	0.0103	53.017
YOG32805T	195.05	-4.79	306	58	195	1	124	123	148	71	0.4003	0.2211	0.0112	0.2257	0.0113	53.660
YOG32806T	195.05	-4.79	306	58	195	1	124	75	146	71	0.4000	0.2203	0.0118	0.2119	0.0118	53.447

- All count rates are in count/second/diode except for the counts under "array." These are in counts/second/array. No background subtraction has been done.
- The rates for the background are based on 401 pixels beginning at the pixel indicated in the column heading.
- The rates for the 0 order spectrum is based on an average of 36 pixels.
- The rate for the spectrum is based on 857 pixels (0-856).
- The rate for the peak of the spectrum is based on 96 pixels (570-665).
- The effect of noisy channels which were not disabled, if any, has been removed from the rates for the background.

File Name	RA	DEC	ℓ^{II}	b^{II}	λ	β	$\lambda_{\odot}$	SEA	ETA	SA	100	600	1100	Peak	spectrum	array
YOG11907T	11.08	-58.46	304	-58	25	-55	151	14	122	124	0.0113	0.0110	0.0129	0.8139	0.2776	26.849
YOG11908T	11.08	-58.46	304	-58	25	-55	151	57	111	124	0.0128	0.0121	0.0128	0.8167	0.2816	27.050
YOG11909T	11.08	-58.46	304	-58	25	-55	151	38	106	124	0.0150	0.0157	0.0172	0.8813	0.2819	28.392
YOG11B07T	13.51	-51.14	301	-65	16	-50	90	120	130	100	0.0111	0.0097	0.0102	0.9917	0.3346	30.076
YOG11B08T	13.51	-51.14	301	-65	16	-50	90	75	145	100	0.0154	0.0142	0.0159	0.8169	0.2745	27.468
YOG11B09T	13.51	-51.14	301	-65	16	-50	90	106	148	100	0.0104	0.0108	0.0120	0.9220	0.3147	28.703
YOG11C07T	17.95	-40.49	287	-76	3	-43	152	50	126	131	0.0095	0.0086	0.0086	0.8817	0.2901	26.141
YOG11C08T	17.95	-40.49	287	-76	3	-43	152	8	125	131	0.0110	0.0111	0.0101	0.8775	0.2920	26.738
YOG11C09T	17.95	-40.49	287	-76	3	-43	152	64	129	131	0.0100	0.0106	0.0096	0.8970	0.3052	27.504
YOG11F07T	40.89	-10.87	186	-59	34	-25	107	130	141	74	0.0084	0.0100	0.0106	1.7639	0.6123	50.783
YOG11F08T	40.89	-10.87	186	-59	34	-25	107	158	128	74	0.0104	0.0099	0.0107	2.0509	0.7287	59.910
YOG11F09T	40.89	-10.87	186	-59	34	-25	107	75	102	74	0.0088	0.0094	0.0109	1.5978	0.5198	43.466
YOG11O07T	85.68	-68.10	278	-31	44	-87	104	34	95	91	0.0130	0.0103	0.0130	1.5739	0.5130	44.560
YOG11O08T	85.68	-68.10	278	-31	44	-87	105	159	98	91	0.0098	0.0090	0.0097	2.5111	0.8791	71.607
YOG11O09T	85.68	-68.10	278	-31	44	-87	105	95	109	91	0.0125	0.0129	0.0129	1.7117	0.6138	52.944
YOG11P07T	123.71	75.97	138	31	103	54	65	72	104	62	0.0096	0.0087	0.0111	1.1294	0.3739	32.868
YOG11P08T	123.71	75.97	138	31	103	54	65	108	103	62	0.0101	0.0109	0.0113	1.6731	0.5871	49.237
YOG11P09T	123.71	75.97	138	31	103	54	65	36	89	62	0.0099	0.0098	0.0114	1.1298	0.3662	32.263
YOG11R07T	140.30	80.28	132	32	104	59	97	152	123	59	0.0088	0.0098	0.0094	1.5300	0.5140	43.187
YOG11R08T	140.30	80.28	132	32	104	59	97	108	111	59	0.0108	0.0101	0.0089	1.5831	0.5884	49.322
YOG11R09T	140.30	80.28	132	32	104	59	97	147	106	59	0.0085	0.0080	0.0093	1.5213	0.5100	42.508
YOG11W07T	150.09	0.54	238	41	151	-10	96	102	153	55	0.0096	0.0108	0.0109	3.2384	1.0334	82.763
YOG11W08T	150.09	0.54	238	41	151	-10	96	166	118	55	0.0095	0.0104	0.0112	3.5231	1.1187	89.192
YOG11W09T	150.09	0.54	238	41	151	-10	96	104	163	55	0.0113	0.0107	0.0116	3.2187	1.0323	82.850
YOG12107T	163.10	38.57	180	62	148	28	339	79	98	149	0.0120	0.0132	0.0124	1.3317	0.4702	42.517
YOG12108T	163.10	38.57	180	62	148	28	339	40	128	149	0.0132	0.0137	0.0147	1.1092	0.3688	34.017
YOG12109T	163.10	38.57	180	62	148	28	339	34	149	149	0.0124	0.0108	0.0113	1.0359	0.3398	30.711
YOG12207T	184.49	33.94	168	79	191	32	63	24	124	102	0.0103	0.0102	0.0108	0.9889	0.3270	29.348
YOG12208T	184.49	33.94	168	79	191	32	63	45	110	102	0.0129	0.0134	0.0125	1.0319	0.3313	30.808
YOG12209T	184.49	33.94	168	79	191	32	63	64	107	102	0.0184	0.0180	0.0166	1.0046	0.3410	33.550
YOG12407T	188.57	13.33	285	75	182	15	335	47	97	149	0.0105	0.0097	0.0112	1.3611	0.4419	37.910
YOG12408T	188.57	13.33	285	75	182	15	335	20	128	149	0.0110	0.0104	0.0128	1.3355	0.4278	37.413
YOG12409T	188.57	13.33	285	75	182	15	335	47	146	149	0.0087	0.0093	0.0104	1.2672	0.4073	34.966
YOG12507T	194.57	30.21	98	86	180	33	139	105	154	50	0.0101	0.0097	0.0124	1.8861	0.5976	50.023
YOG12508T	194.57	30.21	98	86	180	33	139	62	123	50	0.0120	0.0105	0.0107	1.8375	0.5880	49.273
YOG12509T	194.57	30.21	98	86	180	33	139	158	119	50	0.0108	0.0119	0.0100	2.0220	0.6470	53.743
YOG12607T	198.54	70.56	120	46	221	65	2	148	97	107	0.0101	0.0114	0.0121	2.5256	1.0039	83.090
YOG12608T	198.54	70.56	120	46	221	65	2	117	91	107	0.0102	0.0098	0.0109	2.9286	1.1773	97.305
YOG12609T	198.54	70.56	120	46	221	65	2	92	91	107	0.0096	0.0089	0.0097	1.1161	0.4562	39.412
YOG12907T	205.71	71.29	117	45	220	67	1	85	95	106	0.0089	0.0085	0.0085	0.9539	0.3741	33.103
YOG12908T	205.71	71.29	117	45	220	67	1	122	100	106	0.0087	0.0095	0.0094	1.6378	0.6164	51.233
YOG12909T	205.71	71.29	117	45	220	67	1	145	101	106	0.0147	0.0144	0.0162	2.2896	0.9100	77.604
YOG12D07T	215.20	-7.88	337	48	215	5	82	43	137	132	0.0082	0.0113	0.0104	1.3377	0.4402	37.573
YOG12D08T	215.20	-7.88	337	48	215	5	82	31	116	132	0.0091	0.0102	0.0088	1.3933	0.4409	37.383
YOG12D09T	215.20	-7.88	337	48	215	5	82	92	113	132	0.0119	0.0125	0.0113	1.4965	0.5262	45.181
YOG12E07T	217.15	3.57	351	57	213	17	82	44	145	129	0.0073	0.0076	0.0087	1.2411	0.3921	33.165
YOG12E08T	217.15	3.57	351	57	213	17	82	32	119	129	0.0099	0.0089	0.0086	1.1555	0.3846	33.087
YOG12E09T	217.15	3.57	351	57	213	17	82	92	116	129	0.0089	0.0096	0.0085	1.2411	0.4385	37.327
YOG12M07T	326.17	1.75	57	-36	328	14	112	60	152	141	0.0121	0.0118	0.0126	1.1750	0.3908	34.863
YOG12M08T	326.17	1.75	57	-36	328	14	112	94	128	141	0.0116	0.0103	0.0115	1.3050	0.4362	37.878
YOG12M09T	326.17	1.75	57	-36	328	14	112	36	113	141	0.0115	0.0116	0.0112	1.1711	0.3827	33.961
YOG20207T	28.81	56.41	131	-5	49	41	108	154	110	67	0.0092	0.0101	0.0101	2.1477	0.7447	61.113
YOG20208T	28.81	56.41	131	-5	49	41	109	50	106	67	0.0097	0.0104	0.0112	1.4809	0.5052	43.047
YOG20209T	28.81	56.41	131	-5	49	41	109	109	147	67	0.0116	0.0127	0.0123	1.5433	0.5234	45.412
YOG20407T	50.01	49.03	146	-6	61	29	109	126	152	54	0.0101	0.0097	0.0105	2.0717	0.6762	55.657
YOG20408T	50.01	49.03	146	-6	61	29	109	152	132	54	0.0109	0.0094	0.0100	2.3361	0.7936	64.782
YOG20409T	50.01	49.03	146	-6	61	29	109	73	108	54	0.0098	0.0101	0.0099	2.0554	0.6701	55.452
YOG20807T	67.73	59.89	147	7	76	37	154	106	146	80	0.0119	0.0097	0.0103	1.2756	0.4325	37.363
YOG20W07T	162.14	-58.74	287	0	158	-57	343	95	104	114	0.0133	0.0130	0.0157	1.8184	0.6868	58.980
YOG20W08T	162.14	-58.74	287	0	158	-57	343	137	95	114	0.0120	0.0145	0.0149	4.8689	1.8114	144.705
YOG20W09T	162.14	-58.74	287	0	158	-57	343	48	78	114	0.0098	0.0103	0.0115	1.6554	0.6019	50.887
YOG20[illegible]	162.27	-58.68	287	0	158	-57	343	94	105	115	0.0170	0.0158	0.0170	1.8828	0.7160	62.303